
Parallel Tempering With a Variational Reference

Nikola Surjanovic
Department of Statistics
University of British Columbia
nikola.surjanovic@stat.ubc.ca

Saifuddin Syed
Department of Statistics
University of Oxford
saifuddin.syed@stats.ox.ac.uk

Alexandre Bouchard-Côté
Department of Statistics
University of British Columbia
bouchard@stat.ubc.ca

Trevor Campbell
Department of Statistics
University of British Columbia
trevor@stat.ubc.ca

Abstract

Sampling from complex target distributions is a challenging task fundamental to Bayesian inference. Parallel tempering (PT) addresses this problem by constructing a Markov chain on the expanded state space of a sequence of distributions interpolating between the posterior distribution and a fixed reference distribution, which is typically chosen to be the prior. However, in the typical case where the prior and posterior are nearly mutually singular, PT methods are computationally prohibitive. In this work we address this challenge by constructing a generalized annealing path connecting the posterior to an adaptively tuned variational reference. The reference distribution is tuned to minimize the forward (inclusive) KL divergence to the posterior distribution using a simple, gradient-free moment-matching procedure. We show that our adaptive procedure converges to the forward KL minimizer, and that the forward KL divergence serves as a good proxy to a previously developed measure of PT performance. We also show that in the large-data limit in typical Bayesian models, the proposed method improves in performance, while traditional PT deteriorates arbitrarily. Finally, we introduce PT with two references—one fixed, one variational—with a novel split annealing path that ensures stable variational reference adaptation. The paper concludes with experiments that demonstrate the large empirical gains achieved by our method in a wide range of realistic Bayesian inference scenarios.

1 Introduction

Parallel tempering (PT) is a popular approach to sampling from challenging probability distributions used in many scientific disciplines [1–4]. PT methods involve running Markov chain Monte Carlo (MCMC) on the expanded state space of a sequence of distributions that connect the target distribution of interest, π_1 , to a simple reference distribution, π_0 , for which i.i.d. sampling is tractable. The key innovation in PT is that the MCMC chain enables distributions along the path to swap states (or *communicate*). This communication enables i.i.d. draws from the reference π_0 to aid in exploration of the challenging target π_1 . Indeed, recent work has shown that the effectiveness of a PT method is essentially characterized by the efficiency of this communication via the *global communication barrier* (GCB) from π_0 to π_1 [5]. Intuitively, the GCB is low when the reference π_0 is similar to the target π_1 ; in this case, the distributions along the path have substantial overlap and proposed swaps are generally accepted. The GCB is also inversely related to the *restart rate*, which quantifies how frequently i.i.d. samples from π_0 traverse the path to π_1 (a *restart*) [5].

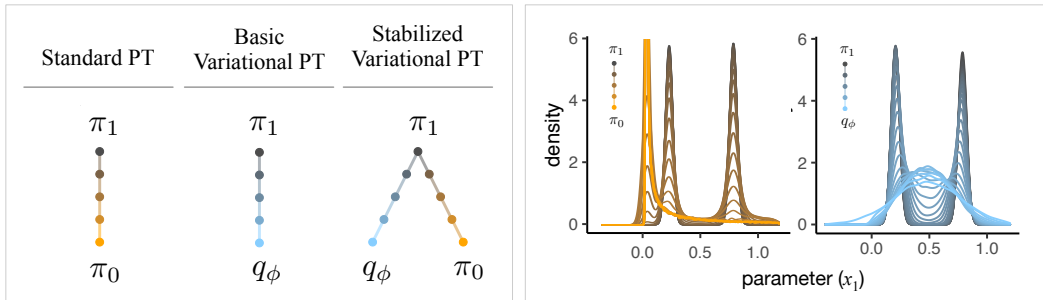


Figure 1: **Left box:** visualization of the three main PT algorithms considered in this work. Nodes represent distributions interpolating between tractable reference distributions (bottom, either fixed π_0 or variational q_ϕ), and an intractable distribution (top, π_1 , typically a Bayesian posterior). Edges encode the structure of the possible swaps performed by the various PT algorithms. **Right box:** examples of a path of marginal distributions obtained on a Bayesian ODE parameter estimation problem with more than one latent variable for an mRNA transfection dataset [4, page 8]. The two modes are non-trivial to switch as they require changing other parameters (not shown) simultaneously. In this example, the marginal of the prior places a small amount of mass on the second mode whereas the marginal of the variational reference places significant mass on both modes. Because the variational reference covers both modes, the length of the annealing path from the reference to the target is shorter and it is easier to obtain samples from the target distribution using parallel tempering.

In the setting of Bayesian posterior inference—a key application of PT, and the focus of this work—the target π_1 is the posterior distribution, and the reference distribution π_0 is typically set to the prior. From the perspective of PT communication efficiency, this is a poor choice in general; the prior is often quite different from the posterior, resulting in a high GCB. As an extreme (but common) example, we show in this work that when the posterior distribution concentrates in the large-data limit, the restart rate with a fixed reference tends to zero and PT becomes computationally infeasible (Proposition 3.1). On the other hand, the posterior often exhibits regularities—asymptotic normality in certain parameters, for example—that motivate the need for a choice of PT reference that can automatically adapt to the target to obtain computational gains.

In this work, we develop and analyze a novel PT algorithm that automatically adapts a variational reference distribution within a parametric family, $\mathcal{Q} = \{q_\phi : \phi \in \Phi\}$. This adaptive reference family addresses the shortcomings of using the prior as a PT reference: we show that in the large-data limit, the restart rate with an appropriate variational reference improves arbitrarily (Proposition 3.2). We find that even when one is not in the large data setting, our method can provide large empirical gains compared to fixed-reference PT in a wide range of realistic Bayesian inference scenarios. The method is based on two major methodological contributions. First, we adapt the parameter ϕ to minimize the forward (inclusive) KL divergence $\text{KL}(\pi_1 \| q_\phi)$ instead of directly taking gradients with respect to the GCB itself. This approach is particularly advantageous when \mathcal{Q} is an exponential family: Theorem 3.5 shows that the forward KL is a good surrogate of the GCB, and minimizing the forward KL amounts to matching moments, which involves no extra tuning effort from the user. We perform moment matching in a simple iterative fashion, in rounds of increasingly many PT draws; Theorem 3.4 identifies conditions that guarantee that the variational parameter estimate converges to the optimum. Second, we combine two references—one fixed, one variational—by “gluing” two PT algorithms together (each based on one of the references, see Fig. 1). We demonstrate that this “stabilized” method is necessary for obtaining a reliable PT algorithm: adaptation with just the variational reference alone can lead to “forgetting” the structure of the posterior distribution (e.g., multi-modality, as shown in Fig. 2). Although this requires more computational effort, we show that under idealized conditions the restart rate of our adaptive method is no lower than half the restart rate of standard, fixed reference PT (Theorem 3.6) after accounting for the doubled computation time. In practice, it is often much better. Finally, the paper presents an extensive empirical study of the performance of our method in a variety of real-world Bayesian models, including spatial models (sparse random field Poisson regression) and functional data analysis (Bayesian estimation of ODE parameters), among others. We find that our method can substantially increase the performance of PT.

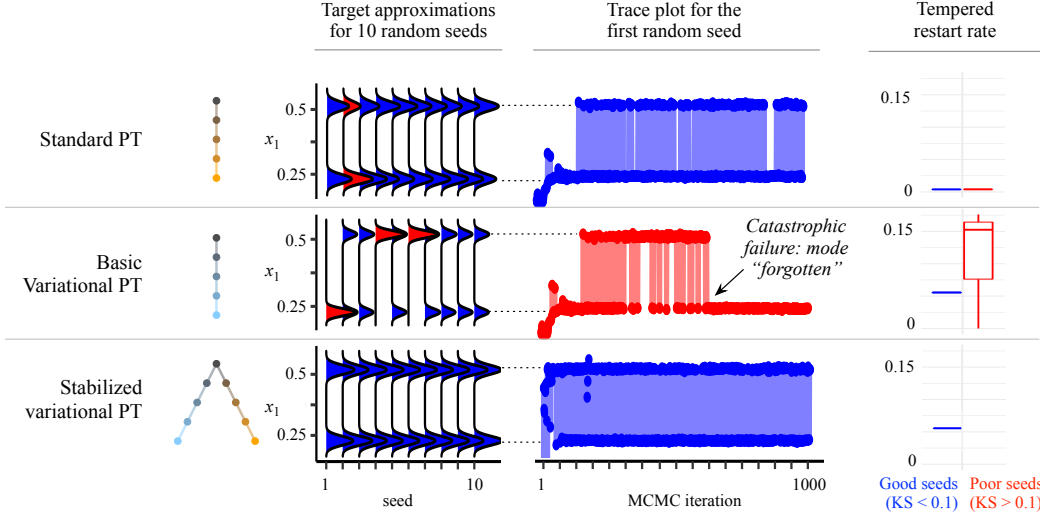


Figure 2: Comparison of three PT methods for Bayesian ODE parameter estimation with an mRNA transfection dataset [4, page 8]. **Top row:** standard PT succeeds in achieving a positive but small restart rate (a measure of PT efficiency; higher is better). **Middle row:** basic implementation of only one variational reference distribution leads to catastrophic failures in 3 out of 10 independent runs. The variational distribution sometimes “forgets” one of the modes (red denotes “bad” approximations with a Kolmogorov-Smirnov distance for the marginal posterior over the model parameter x_1 larger than 0.1) and becomes stuck in the other, which leads to an overestimation of the restart rate. **Bottom row:** using both a fixed and an adaptive reference addresses this issue and leads to markedly better performance in terms of restart rate compared to standard PT. All methods have a comparable cost per iteration; all use the same variational reference family and run the same total number of chains and iterations.

Related work. The idea of adapting the tractable end-point of a path of distributions has been explored most thoroughly in the context of estimation of normalization constants [6–9]. However, the importance of having both a fixed and adaptive reference has not appeared in this literature. In the PT literature, the closest related work appears to be [10, section 5] and [11, section 4.1], which consider PT algorithms with non-prior references. However, no adaptive algorithm is proposed; the reference distribution is set to a fixed variational approximation in [10] and to a Gaussian approximation at an analytically tractable mode in [11]. Reference adaption has been considered in passing in the annealed importance sampling and sequential Monte Carlo literature, but without carefully considering the importance of stabilization discussed in our work, e.g. [12]. Another related line of work is the design of adaptive independence Metropolis-Hastings (IMH) proposals [13–16]. In particular, the theoretical work studying convergence of adaptive IMH has recognized the usefulness of combining the adaptive reference with a fixed reference [17, Section 7]. However, compared to the PT context, this combination is more straightforward to achieve in IMH via alternation of samplers. Finally, variational inference has previously been used to aid Monte Carlo methods, e.g., to learn proposals in sequential Monte Carlo [18], annealed importance sampling [19], and MCMC [20], and to form an initial reference for MCMC [21, 22]. None of these works connect the KL objective directly to the performance of a PT algorithm as we do in this paper.

2 Background

This work builds on a recent state-of-the-art PT method, non-reversible parallel tempering (NRPT) [5]. The goal is to sample from a target distribution, π_1 , on a state space \mathcal{X} . This is achieved by constructing a sequence of $N + 1$ distributions from π_1 to a reference distribution π_0 also on \mathcal{X} . Given an *annealing schedule* $\mathcal{B}_N = (\beta_n)_{n=0}^N$, where $0 = \beta_0 < \beta_1 < \dots < \beta_N = 1$ with mesh size $\|\mathcal{B}_N\| = \max_n |\beta_n - \beta_{n-1}|$, the distribution for each chain $n = 0, \dots, N$ is given by π_{β_n} , where for all $\beta \in [0, 1]$, $\pi_\beta(x) \propto \pi_0^{1-\beta}(x) \cdot \pi_1^\beta(x)$.

Algorithm 1 Non-reversible parallel tempering (NRPT)

Require: Initial state \mathbf{x}_0 , annealing schedule \mathcal{B}_N , # iterations T , annealing path π_β

```

 $r_n \leftarrow 0$  for  $n = 0, 1, \dots, N - 1$ 
for  $t = 1, 2, \dots, T$  do
   $\mathbf{x} \leftarrow \text{LocalExploration}(\mathbf{x}_{t-1})$  ▷ Local exploration kernels (e.g., HMC)
   $S_t \leftarrow$  if  $t$  is even  $S_{\text{even}}$  else  $S_{\text{odd}}$ 
  for  $n = 0, 1, \dots, N - 1$  do
     $\alpha_n \leftarrow \alpha_n(\mathbf{x})$  ▷ Acceptance probability from (1)
     $r_n \leftarrow r_n + (1 - \alpha_n)/T$  ▷ Store chain communication rejection rate estimates
     $U_n \leftarrow \text{Unif}(0, 1)$ 
    if  $n \in S_t$  and  $U_n \leq \alpha_n$  then  $x^{n+1}, x^n \leftarrow x^n, x^{n+1}$  ▷ Swap components  $n$  and  $n + 1$  of  $\mathbf{x}$ 
  end for
   $\mathbf{x}_t \leftarrow \mathbf{x}$ 
end for
Return:  $(\mathbf{x}_t)_{t=1}^T, (r_n)_{n=0}^{N-1}$ 

```

In parallel tempering, we simulate a Markov chain $\mathbf{X}_t = (X_t^0, \dots, X_t^N)$ that targets the product distribution π on \mathcal{X}^{N+1} given by $\pi(\mathbf{x}) = \pi_{\beta_0}(x^0) \cdot \pi_{\beta_1}(x^1) \cdots \pi_{\beta_N}(x^N)$ as the unique invariant probability distribution of the Markov chain. Note that the target distribution π_1 is a marginal of π , hence Monte Carlo averages based on X_t^N converge to the correct posterior expectations. Each iteration of PT involves two steps—*local exploration* and *communication*—as shown in Algorithm 1. The local exploration step involves applying, for each chain n , a π_{β_n} -invariant Markov kernel (e.g. Hamiltonian Monte Carlo). The communication step involves Metropolized swaps of states between adjacent chains; one alternates between swaps of chains n and $n+1$ for all n in S_{even} followed by S_{odd} , where S_{even} and S_{odd} are the even and odd subsets of $\{0, \dots, N - 1\}$, respectively. The deterministic alternation between even and odd swaps enjoys remarkable theoretical and empirical properties and ensures that the performance of parallel tempering does not degrade as N increases [5]. Each proposed swap of component n and $n + 1$ of $\mathbf{x} = (x^0, \dots, x^N)$ is accepted or rejected independently with probability

$$\alpha_n(\mathbf{x}) = 1 \wedge \frac{\pi_{\beta_n}(x^{n+1}) \cdot \pi_{\beta_{n+1}}(x^n)}{\pi_{\beta_n}(x^n) \cdot \pi_{\beta_{n+1}}(x^{n+1})}. \quad (1)$$

To characterize the performance of a parallel tempering method we study how often samples *restart*, i.e. travel from the reference π_0 to the target π_1 [5]. Studying restarts isolates the effect of communication from the problem-specific characteristics of local exploration. (An improved local exploration kernel will of course improve overall performance.) When it is possible to obtain i.i.d. samples from π_0 , the number of restarts is empirically found to be related to the effective sample size in the target distribution chain [5]. Formally, the *restart rate* $\tau(\mathcal{B}_N)$ from π_0 to π_1 with schedule \mathcal{B}_N is the fraction of PT iterations that result in a restart. The maximum value of τ is $1/2$, since a communication swap is proposed with π_0 at every other iteration of PT. If the local exploration is efficient (Assumption A.2) then $\tau(\mathcal{B}_N) = (2 + 2 \sum_{n=0}^{N-1} \frac{r_n}{1-r_n})^{-1}$ [5, Corollary 1], where $r_n = 1 - \mathbb{E}[\alpha_n(\mathbf{X})]$ and $\mathbf{X} \sim \pi$. Asymptotically as $N \rightarrow \infty$, the round trip rate converges to a constant known as the *asymptotic restart rate* τ : $\lim_{\|\mathcal{B}_N\| \rightarrow 0} \tau(\mathcal{B}_N) = \tau = (2 + 2\Lambda(\pi_0, \pi_1))^{-1}$ [5, Theorem 3], where $\Lambda(\pi_0, \pi_1)$ is the *global communication barrier* (GCB) between π_0 and π_1 ,

$$\Lambda(\pi_0, \pi_1) = \frac{1}{2} \int_0^1 \mathbb{E}[|\ell(X_\beta) - \ell(X'_\beta)|] d\beta, \quad \ell(x) = \log \frac{\pi_1(x)}{\pi_0(x)}, \quad X_\beta, X'_\beta \stackrel{\text{i.i.d.}}{\sim} \pi_\beta. \quad (2)$$

The GCB can be estimated using the rejection rates r_n for all adjacent pairs of chains, $\Lambda(\pi_0, \pi_1) \approx \sum_{n=0}^{N-1} r_n$, where $r_n = 1 - \mathbb{E}[\alpha_n(\mathbf{X})]$ for $\mathbf{X} \sim \pi$, with the approximation error decreasing to zero at a rate $O(N^{-2})$ as the number of chains N increases [5, Section 5.2]. GCB values near zero imply that swaps are typically accepted and communication is efficient.

3 Parallel tempering with a variational reference

A key degree of freedom one has when using PT is the reference distribution, π_0 . Although the standard approach is to set π_0 to the prior, Eq. (2) suggests that the GCB might be quite large—and

hence communication performance quite poor—when the prior and posterior differ significantly, which commonly occurs in practice. Indeed, Proposition 3.1 motivates the importance of choosing the reference carefully: in a typical Bayesian model, as one obtains more data, the restart rate for the prior reference tends to zero. This result relies on Assumption B.3 in Appendix B, which stipulates standard technical conditions sufficient for, e.g., asymptotic consistency of the MLE, a Bernstein-von Mises result for asymptotic normality of the posterior [23], along with PT-specific assumptions such as efficient local exploration. We emphasize this result is a motivation for our methodology; the proposed algorithms apply much more broadly and not only in the data limit.

Proposition 3.1 (Large-data restart rate, fixed reference). *Consider data $\mathbf{Y}_m = \{Y_i\}_{i=1}^m$ generated i.i.d. from a model with likelihood $L(y|x_0)$, $x_0 \in \mathcal{X} \subset \mathbb{R}^d$, satisfying the conditions in Assumption B.3. Denote $\pi_{1,m}$ to be the posterior conditioned on \mathbf{Y}_m . Then, in the large-data limit, the asymptotic restart rate τ_m associated with the annealing path from π_0 to $\pi_{1,m}$ degrades arbitrarily, i.e., $\tau_m \rightarrow 0$ almost surely as $m \rightarrow \infty$.*

In this section, we demonstrate that allowing the reference to be *tunable* addresses this issue.

3.1 Annealing paths with a variational reference

Let $\mathcal{Q} = \{q_\phi : \phi \in \Phi\}$ be a parametric family of distributions on \mathcal{X} , and for each $\phi \in \Phi$, denote the annealing path from the reference distribution q_ϕ to the target π_1 by

$$\forall \beta \in [0, 1], \quad \pi_{\phi,\beta}(x) \propto q_\phi(x)^{1-\beta} \cdot \pi_1(x)^\beta.$$

Note that for this modified annealing path, the target distribution π_1 remains the same although the reference may change. In the Bayesian framework, this means that the prior π_0 and posterior π_1 remain the same while the variational reference q_ϕ is tuned. To ensure the variational reference family \mathcal{Q} is compatible with the asymptotic PT theory developed in [5], we will assume \mathcal{Q} is a *PT-suitable family* for the target π_1 , i.e., each $q_\phi \in \mathcal{Q}$ shares the same support at the target and satisfies some mild moment conditions (Assumption A.1 in Appendix A). We will also assume throughout that the fixed reference π_0 is itself *PT-suitable* for π_1 . PT-suitability is sufficient to guarantee that the restart rate is inversely related to the GCB and that the schedule-tuning procedure from [5, Section 5.4] is justified.

3.2 Exponential variational reference family

The variational reference family \mathcal{Q} should be flexible enough to match the target π_1 reasonably well, but also simple enough to enable i.i.d. sampling, pointwise evaluation, and tractable optimization. Proposition 3.2 suggests that in the large-data limit, the family of multivariate Gaussian distributions often suffices. In particular, unlike the fixed prior reference—whose restart rate decays to zero in the large-data limit—there exists a sequence of multivariate normal reference distributions so that the restart rate tends to its maximum value of $1/2$. Note again that this large-data setting is just one instance in which a tunable reference helps; our method in this work applies much more broadly, and does not require a Gaussian reference or rely on the asymptotic setup in Proposition 3.2. In particular, our method is advantageous in any setting where the GCB decreases compared to fixed-reference PT.

Proposition 3.2 (Large-data restart rate, variational reference). *Consider the setting of Proposition 3.1, and suppose $\mathcal{Q} = \{\mathcal{N}(\mu, \Sigma) : \mu \in \mathbb{R}^d, \Sigma \in \mathbb{R}^{d \times d}, \Sigma = \Sigma^\top \succ 0\}$ is a PT-suitable family for all targets $\pi_{1,m}$ almost surely. Then for any fixed $N > 1$, there exists a random sequence $\mu_m \in \mathbb{R}^d$, $\Sigma_m \in \mathbb{R}^{d \times d}$ such that for any schedule \mathcal{B}_N , in the large-data limit, the restart rate $\tau_m(\mathcal{B}_N)$ associated with $\pi_{1,m}$, $\mathcal{N}(\mu_m, \Sigma_m)$ converges to the maximum possible value. I.e., for any schedule \mathcal{B}_N we have $\tau_m(\mathcal{B}_N) \xrightarrow{P} 1/2$ as $m \rightarrow \infty$.*

Proposition 3.2 motivates the use of a tunable variational reference that can adapt to the target, as opposed to a fixed reference. In this work, we consider the general class of exponential reference families of full-rank where the distributions take the form $q_\phi(x) = h(x) \exp(\phi^\top \eta(x) - A(\phi))$, for base density h , natural parameter ϕ , sufficient statistic η , and log partition function A . Aside from being flexible enough to match posteriors arbitrarily well in the large-data limit, a key advantage of an exponential reference family is that it is straightforward to fit: one can obtain the forward (inclusive) KL divergence minimizer $q_{\phi_{\text{KL}}}$ using a simple gradient-free moment matching procedure because $\mathbb{E}_{\phi_{\text{KL}}}[\eta] = \mathbb{E}_1[\eta]$, where \mathbb{E}_ϕ and \mathbb{E}_1 denote expectations with respect to q_ϕ and π_1 , respectively [24].

Indeed, under slightly more stringent technical assumptions in the setting of Propositions 3.1 and 3.2—namely Assumption B.9—Proposition 3.3 shows that we may use this forward KL fit as the reference sequence $\mathcal{N}(\mu_m, \Sigma_m)$ for which the restart rate is asymptotically maximized. Assumption B.9 stipulates that the differences between the posterior mean and MLE, as well as between the inverse Fisher information and scaled posterior variance, are not too large.

Proposition 3.3 (Large-data restart rate, moment matched reference). *Consider the setting of Proposition 3.2 and suppose that Assumption B.9 also holds. Then, the conclusion of Proposition 3.2 holds if μ_m, Σ_m are set to the mean and variance of $\pi_{1,m}$ conditioned on \mathbf{Y}_m , respectively.*

3.3 Tuning the variational reference

In practice, we fit the exponential family reference iteratively by running NRPT for multiple tuning rounds $r = 1, \dots, R$; in each tuning round r we run $T_r = 2^r$ iterations with variational parameter $\hat{\phi}_r$. Using the generated states $(\mathbf{X}_{t,r})_{t=1}^{T_r}$, we obtain the parameter $\hat{\phi}_{r+1}$ for round $r + 1$ by solving

$$\mathbb{E}_{\hat{\phi}_{r+1}}[\eta] = \frac{1}{T_r} \sum_{t=1}^{T_r} \eta(X_{t,r}^N). \quad (3)$$

Note that by relying on sufficient statistics, we are not required to keep in memory the MCMC trace or to loop over MCMC samples when performing variational parameter optimization. For example, when \mathcal{Q} is a Gaussian family, Eq. (3) simplifies to setting the mean vector and covariance matrix to the empirical mean and covariance obtained from the target chain samples $X_{t,r}^N$. When a full (non-diagonal) covariance matrix is used, one should start tuning when $T_r \geq d$. We additionally use the samples from each round to tune the annealing schedule \mathcal{B}_N using the procedure from [5].

Theorem 3.4 shows that if the absolute spectral gap $\text{Gap}(\phi)$ [25] of the PT Markov chain with reference q_ϕ is bounded away from zero, and the number of iterations in each round tends to infinity at an appropriate rate, then $\hat{\phi}_r$ will converge almost surely to the forward KL minimizer ϕ_{KL} . Although Theorem 3.4 stipulates that η is bounded, this is a technicality that is not required in practice.

Theorem 3.4 (Convergence of variational reference tuning). *Suppose $\mathcal{Q} = \{q_\phi : \phi \in \Phi\}$ is a PT-suitable exponential family of full rank with sufficient statistic $\eta(x)$ bounded in x . Further assume that ϕ_{KL} exists and is unique. Suppose each round of tuning starts at stationarity and there is $\kappa > 0$ such that $\text{Gap}(\phi) \geq \kappa > 0$ for all ϕ and $T_r = \Omega(2^r)$ as $r \rightarrow \infty$. Then, (1): $\hat{\phi}_r \rightarrow \phi_{\text{KL}}$ almost surely as $r \rightarrow \infty$; and (2): for all $0 < \epsilon < \frac{1}{2}$, almost surely there exists an $R(\epsilon)$ such that for all $r \geq R(\epsilon)$, $\|\mathbb{E}_{\hat{\phi}_r}[\eta] - \mathbb{E}_1[\eta]\| \leq T_r^{-\frac{1}{2} + \epsilon}$.*

3.4 Forward KL as a surrogate objective

We now provide a general theoretical justification for the minimization of the forward KL divergence as opposed to the global communication barrier, which is appealing as it enables a simple gradient-free moment matching procedure. First, note that when $\pi_1 \in \mathcal{Q}$, minimizing the KL divergence and the GCB is equivalent since they are both divergences [5]. Theorem 3.5 generalizes this to the more usual case where $\pi_1 \notin \mathcal{Q}$, demonstrating that the GCB at the forward KL minimum is bounded by quantities that depend on the flexibility of the variational family. In particular, provided that there exists a $\phi_0 \in \Phi$ such that the difference between log densities of the target π_1 and reference q_{ϕ_0} is bounded by a function g , then the GCB evaluated at the forward KL minimizer is bounded by a term involving expectations of g under the target and distributions q_ϕ that are close to π_1 .

Theorem 3.5 (Forward KL proxy for the GCB). *Suppose that $\mathcal{Q} = \{q_\phi : \phi \in \Phi\}$ is a PT-suitable exponential family of full rank. Let g be any function such that for some $\phi_0 \in \Phi$ and for all $x \in \mathcal{X}$, $|\log \pi_1(x) - \log q_{\phi_0}(x)| \leq g(x)$. Then, if $\phi_{\text{KL}} = \arg \min_\phi \text{KL}(\pi_1 \| q_\phi)$ exists and is unique, we have that $\Lambda(q_{\phi_{\text{KL}}}, \pi_1) \leq \sqrt{\frac{1}{2} (\mathbb{E}_1[g] + \sup_{\phi \in \Phi'} \mathbb{E}_\phi[g])}$, where $\Phi' = \{\phi : \text{KL}(\pi_1 \| q_\phi) \leq \text{KL}(\pi_1 \| q_{\phi_0})\}$.*

We consider in Appendix D two simple examples to verify that the upper bound given by Theorem 3.5 is small enough for practical purposes.

Algorithm 2 Variational PT

Require: initial state \mathbf{x}_0 , # chains $\bar{N} = 2N$, # total tuning rounds R , target π_1 , reference family $\mathcal{Q} = \{q_\phi : \phi \in \Phi\}$, initial reference parameter ϕ , fixed reference π_0
 $\mathcal{B}_{\phi,N}, \mathcal{B}_N \leftarrow (0, 1/N, 2/N, \dots, 1)$ \triangleright Initialize annealing parameters uniformly with $N_\phi = N$
for $r = 1, 2, \dots, R$ **do**
 $T \leftarrow 2^r$ \triangleright Double the number of iterations in the next tuning round
 $\bar{\pi}_{\phi,\beta} \leftarrow \text{Concatenate}(\pi_{\phi,\beta}, \pi_\beta)$ \triangleright Concatenate paths using (4)
 $\bar{\mathcal{B}}_{\phi,\bar{N}} \leftarrow \text{Concatenate}(\mathcal{B}_{\phi,N}, \mathcal{B}_N)$ \triangleright Concatenate schedules using (5)
 $(\mathbf{x}_t)_{t=1}^T, (r_n)_{n=0}^{\bar{N}-1} \leftarrow \text{NRPT}(\mathbf{x}_0, \bar{\mathcal{B}}_{\phi,\bar{N}}, T, \bar{\pi}_{\phi,\beta})$ \triangleright PT with two references
 $\mathcal{B}_{\phi,N} \leftarrow \text{UpdateSchedule}((r_n)_{n=0}^{\bar{N}-1}, \mathcal{B}_{\phi,N})$ \triangleright Tune annealing parameters for π_ϕ [5]
 $\mathcal{B}_N \leftarrow \text{UpdateSchedule}((r_n)_{n=\bar{N}-1}^N, \mathcal{B}_N)$ \triangleright Tune annealing parameters for π [5]
 $\mathbf{x}_0 \leftarrow \mathbf{x}_T$ \triangleright Initialization for next round
 $\phi \leftarrow \text{UpdateReference}((\mathbf{x}_t)_{t=1}^T)$ \triangleright Tune according to Eq. (3) or another procedure
end for
Return: $(\mathbf{x}_t)_{t=1}^T$

3.5 Stabilization with a fixed reference

In Section 3.3 we provided a result (Theorem 3.4) guaranteeing convergence of the adaptive scheme assuming the existence of an absolute spectral gap. In practice, the risk is that certain regions of Φ may significantly degrade the absolute spectral gap under the basic variational scheme discussed so far. For example, as shown in Fig. 2 (middle row), if the posterior is multimodal, the variational reference may quickly center on one mode; because subsequent rounds of tuning use samples that depend on the variational reference, these samples may largely come from that one mode, causing the variational reference to remain trapped there for many tuning rounds.

To address this issue, we introduce parallel tempering with two reference distributions, using both the original (fixed) reference and a variational reference, which we call “stabilized variational PT”, illustrated in Fig. 1. We create an annealing path that starts at q_ϕ , proceeds along an annealing path to π_1 , and then moves on a new path from π_1 to π_0 , connecting all three distributions. This modification adds significant robustness; as long as there are some restarts from the fixed reference, the target chain will escape the local optima and provide a more accurate estimate of π_1 used to tune q_ϕ . In general, a well-tuned variational reference can provide a significant reduction in GCB compared to just a fixed path, but keeping the fixed reference ensures that the method will never do significantly worse than standard NRPT even if the variational reference tuning performs poorly (Theorem 3.6 below). Our variational PT algorithm with two references is presented in Algorithm 2, in which `UpdateSchedule` refers to [5, Algorithms 2, 3].

To formalize the notion of a piecewise path, let $\pi_{\phi,\beta}$ be the annealing path between q_ϕ and π_1 , and let π_β be the annealing path between the fixed reference π_0 and π_1 . We define the concatenated (piecewise) path $\bar{\pi}_{\phi,\beta}$,

$$\bar{\pi}_{\phi,\beta} = \begin{cases} \pi_{\phi,2\beta} & 0 \leq \beta \leq \frac{1}{2}, \\ \pi_{2-2\beta} & \frac{1}{2} \leq \beta \leq 1. \end{cases} \quad (4)$$

This new annealing path can be used within the NRPT Algorithm 1 as any other path. To tune the annealing schedule within each leg of PT with two references, we define the schedules $\mathcal{B}_{\phi,N_\phi} = (\beta_{\phi,n})_{n=0}^{N_\phi}$ and $\mathcal{B}_N = (\beta_n)_{n=0}^N$ for the legs connecting q_ϕ and π_0 to π_1 , respectively. Then, we define the concatenated schedule $\bar{\mathcal{B}}_{\phi,\bar{N}} = (\bar{\beta}_{\phi,n})_{n=0}^{\bar{N}}$ where $\bar{N} = N_\phi + N$ and

$$\bar{\beta}_{\phi,n} = \begin{cases} \frac{1}{2}\beta_{\phi,n} & 0 \leq n \leq N_\phi \\ 1 - \frac{1}{2}\beta_{\bar{N}-n} & N_\phi \leq n \leq \bar{N} \end{cases} \quad (5)$$

This concatenated schedule $\bar{\mathcal{B}}_{\phi,\bar{N}}$ and path $\bar{\pi}_{\phi,\beta}$ are provided as input to the NRPT algorithm.

Finally, we provide an analysis of the worst-case performance of variational PT with two reference distributions. We show that the asymptotic restart rate of PT with two references is always greater than or equal to the restart rate with either one of the two references alone. Because PT with two references requires twice the amount of computation, this amounts to a worst case of half the performance of regular PT with a fixed reference. In practice we often find that including a variational reference substantially improves the PT restart rate.

Let $\bar{\tau}(\bar{\mathcal{B}}_{\phi, \bar{N}})$ be the restart rate for π_1 for the concatenated path, i.e. the rate at which samples from either reference q_ϕ or π_0 reach the target π_1 . Theorem 3.6 shows that if the Markov chain *efficiently explores locally* (Assumption A.2), then the restart rate of multiple-reference PT is the sum of the restart rate for π_1 between q_ϕ and π_0 denoted $\tau_\phi(\mathcal{B}_{\phi, N_\phi})$ and $\tau(\mathcal{B}_N)$ respectively.

Theorem 3.6 (Restart rate of NRPT with two reference distributions). *Let q_ϕ, π_0 be PT-suitable references for the target π_1 . Suppose the PT chains with references q_ϕ, π_0 with schedules $\mathcal{B}_{\phi, N_\phi}, \mathcal{B}_N$ respectively efficiently explore locally (see Assumption A.2). Then $\bar{\tau}_\phi(\bar{\mathcal{B}}_{\phi, \bar{N}}) = \tau_\phi(\mathcal{B}_{\phi, N_\phi}) + \tau(\mathcal{B}_N)$. Moreover, if $\|\bar{\mathcal{B}}_{\phi, \bar{N}}\| \rightarrow 0$, then*

$$\lim_{\bar{N} \rightarrow \infty} \bar{\tau}_\phi(\bar{\mathcal{B}}_{\phi, \bar{N}}) = \frac{1}{2 + 2\Lambda(q_\phi, \pi_1)} + \frac{1}{2 + 2\Lambda(\pi_0, \pi_1)}.$$

4 Experiments

We consider various Bayesian inference problems: 11 based on real data, and 4 based on synthetic data (see Table 1 in Appendix F for the details of each). The range of problem settings considered include spatial statistics, Bayesian ODE parameter inference, phylogenetic inference, and several distinct Bayesian hierarchical models. In all examples the variational reference is a multivariate normal distribution with either a diagonal estimated covariance matrix (`VPT_diag`) or a full covariance matrix (`VPT_full`). The code for the experiments is made publicly available: Julia code is available at <https://github.com/UBC-Stat-ML/VariationalPT> and Blang code is at <https://github.com/UBC-Stat-ML/bl-vpt-nextflow>. A distributed implementation is also under development at <https://github.com/Julia-Tempering/Pigeons.jl>. Experimental details can be found in Appendix F.

4.1 Comparative efficiency of variational PT families and a PT baseline

We begin by comparing the communication efficiency of both `VPT_diag` and `VPT_full` to a state-of-the-art existing PT method, NRPT [5], which uses a single, fixed reference. Note that there is also a computational trade-off between the two variational families (but we remind the reader that both still yield convergence of the target chain to the posterior). In particular, `VPT_full` offers more flexibility—and hence a potentially lower GCB—at the cost of a higher computational cost per iteration and more variational parameters to fit, while `VPT_diag` has the same asymptotic computational cost per iteration as standard PT methods. We explore this tradeoff in Fig. 3.

We observe that both `VPT_diag` and `VPT_full` often substantially improve the restart rate compared to the NRPT baseline, and at worst achieve similar performance. The choice between `VPT_full` and `VPT_diag` depends on the problem: for example, in low-dimensional problems such as `Challenger` and `Simple-mix`, we observe that the full covariance in `VPT_full` is worth its additional cost per iteration. The situation is reversed in the `Transfection` problem. If one is pressed to select one PT variational family, we recommend `VPT_diag` as a safe default in light of Theorem 3.6 and of its computational cost per iteration asymptotically equivalent to NRPT.

We also note that the tuning procedure converges relatively quickly. We show the number of restarts for the first 2.5% of computation time as insets in Fig. 3, and find that the number of restarts for the three methods can be distinguished early on. We also show in Fig. 4(a) that the GCB estimates converge in a small number of rounds for two additional representative problems (`Lip Cancer` and `Vaccines`). Note also that the GCB is substantially lower when a variational reference is introduced.

4.2 Moment matching outperforms stochastic optimization

Next, we compare the proposed moment matching procedure described in Section 3 to several other stochastic optimization schemes to tune the variational reference. In contrast to moment matching—which is free of tuning hyper-parameters—we show in Appendix F.11.2 that stochastic optimization schemes require extensive hyper-parameter tuning, including step size schedule, choice of optimizer, and surrogate objective function. Moreover, we show in Fig. 5 (left) that it is difficult to specify a “default” hyper-parameter setting for stochastic optimization methods; a setting that works well on one problem (`Rocket`) generally will not work well on other problems (e.g., `Change Point`, `Titanic`). In contrast, moment matching performed well on all 14 problems we considered without requiring tuning. Consequently, our moment matching procedure is a better candidate for integration

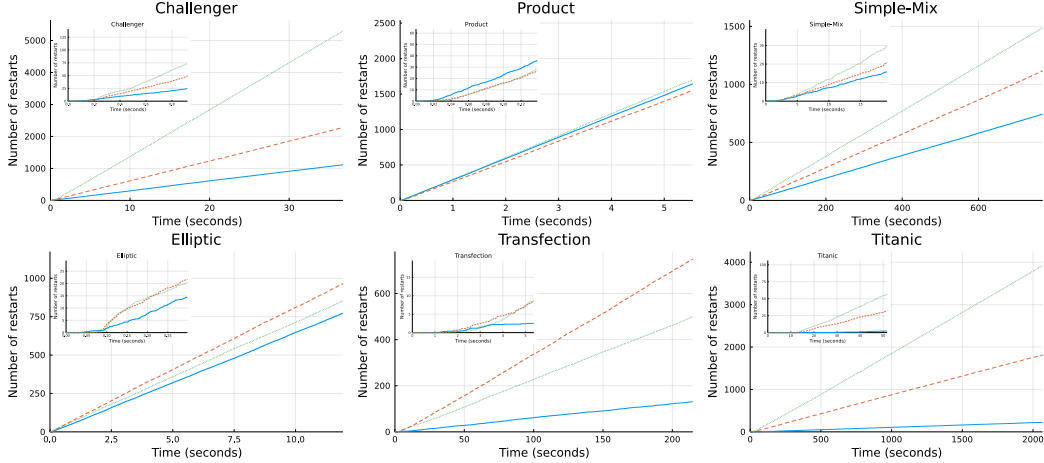


Figure 3: Number of restarts (higher is better) versus computation time in seconds for several models, with **VPT_full** in green, **VPT_diag** in red, and the **NRPT** baseline in blue. The two variational PT methods generally provide a comparable or better rate of restarts per second. Insets highlight the initial 2.5% of computation time, demonstrating that tuning of the variational references stabilizes quickly.

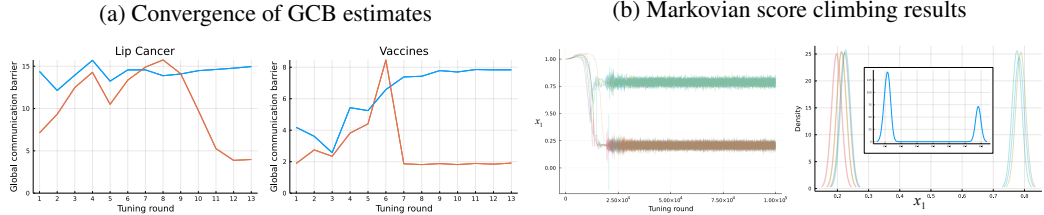


Figure 4: **(a)** GCB for **VPT_diag** (red) and **NRPT** (blue) versus tuning round. **(b, left)** Tuning variational parameters using MSC with 10 replications (colours). The mean of the variational distribution for the model parameter x_1 in the **Transfection** model is presented. The true marginal posterior distribution of x_1 is bimodal (Fig. 2). We see here that MSC chooses one of the two modes for the estimation of the mean parameter. **(b, right)** Variational Gaussian approximation of the same parameter in the **Transfection** model produced by 10 MSC runs with different seeds (colours). The aggregate of the different runs is shown as an inset, cf. Fig. 2.

in probabilistic programming languages (PPLs), in which users do not expect to be required to frequently change algorithmic tuning hyper-parameters. To illustrate this point, we have extended an existing open source PPL, Blang [26], to include our method tuned via moment matching (code available at <https://github.com/UBC-Stat-ML/bl-vpt>).

4.3 Comparison to an externally tuned reference

We also compare our moment-matching variational reference tuning procedure to a reference tuned by an existing procedure outside of the PT context. In particular, we tested Markovian score climbing (MSC) [27]—which also optimizes the forward KL—for tuning a Gaussian reference with a diagonal covariance. Details of MSC tuning, including sensitivity to stochastic optimization settings, can be found in Appendix F.11. The results for the **Transfection** model are presented in Fig. 4. In contrast to our stabilized moment matching approach (Fig. 2), tuning the reference using MSC in this example results in systematic catastrophic forgetting of one of the modes (Fig. 4 (b)) in all 10 replicates. We additionally refer readers to [28] for recent developments in score-based methods to minimize the forward KL divergence.

4.4 Comparison of variational PT topologies

Finally, we compare the three algorithms introduced in Fig. 1 (Basic Variational PT, Stabilized Variational PT and NRPT) on nine Bayesian inference problems (see Fig. 5, right). We set up the algorithms so that the runtime per PT iteration has the same asymptotic complexity:

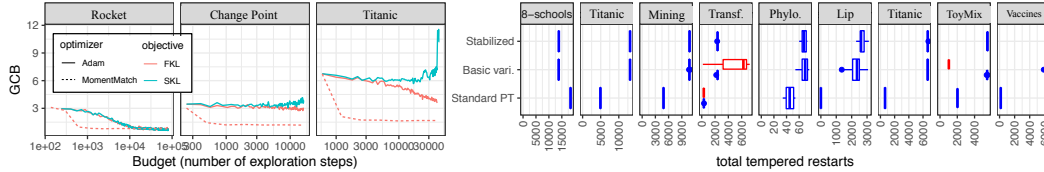


Figure 5: **Left:** comparison of stochastic optimization and moment matching. An optimizer parameter setting that works well for the `Rocket` problem (Adam+FKL/SKL, step size scale 0.1) does not generalize well to other problems (`Change-Point`, `Titanic`). In contrast, moment matching reliably finds a well-tuned reference in all 14 problems considered in this paper. **Right:** the same plot as in Fig. 2, but on a larger selection of models.

this is done by selecting a diagonal covariance matrix for the Gaussian variational family and using the same total number of chains for all methods.

The results confirm the initial findings of Fig. 2: only the stabilized method always avoids catastrophic forgetting of modes. Moreover, in all but one example considered, we find that `Stabilized Variational PT` exhibits improved performance in terms of the number of restarts compared to the NRPT baseline (Fig. 5). The exception is the `8-schools` problem, in which the posterior is not well approximated by a diagonal Gaussian. Even in this case, as suggested by Theorem 3.6, the performance does not degrade by more than a factor two. At the other end of the spectrum, for the `Vaccines` hierarchical model, the number of restarts increases >40-fold compared to the NRPT baseline, and for the spatial sparse conditional auto-regressive (CAR) model applied to the `Lip Cancer` problem, the performance jumps from zero restarts to >2300 restarts.

More results and details can be found in Appendix F.11.3, including alternative topological arrangements of variational PT algorithms, effective sample size per second results, as well as global communication barriers for the problems considered in this section.

5 Conclusion

This paper addressed sampling from a complex target distribution within the parallel tempering framework by constructing a generalized annealing path connecting the posterior to an adaptively tuned variational reference. Experiments in a wide range of realistic Bayesian inference scenarios demonstrate the large empirical gains achieved by our method. Potential future work includes extending the gradient-free tuning methodology to larger classes of variational families for the reference distribution. Further, heavy-tailed distributions can violate Assumption A.1 and it is not clear without further examination what the implications are on the convergence of the proposed algorithms. Therefore, another possible direction for future work is to develop methods suitable for heavy-tailed target distributions.

Acknowledgements

NS acknowledges the support of a Vanier Canada Graduate Scholarship. ABC and TC acknowledge the support of an NSERC Discovery Grant. We also acknowledge use of the ARC Sockeye computing platform from the University of British Columbia.

References

- [1] Kazunori Akiyama, Antxon Alberdi, Walter Alef, Juan Carlos Algaba, Richard Anantua, Keiichi Asada, Rebecca Azulay, Uwe Bach, Anne-Kathrin Baczko, David Ball, et al. First Sagittarius A* Event Horizon Telescope results. IV. Variability, morphology, and black hole mass. *The Astrophysical Journal Letters*, 930(2):L15, 2022.
- [2] Kazunori Akiyama, Juan Carlos Algaba, Antxon Alberdi, Walter Alef, Richard Anantua, Keiichi Asada, Rebecca Azulay, Anne-Kathrin Baczko, David Ball, Mislav Baloković, et al. First M87 Event Horizon Telescope results. VII. Polarization of the ring. *The Astrophysical Journal Letters*, 910(1):L12, 2021.

- [3] David J Earl and Michael W Deem. Parallel tempering: theory, applications, and new perspectives. *Physical Chemistry Chemical Physics*, 7(23):3910–3916, 2005.
- [4] Benjamin Ballnus, Sabine Hug, Kathrin Hatz, Linus Görlitz, Jan Hasenauer, and Fabian J Theis. Comprehensive benchmarking of Markov chain Monte Carlo methods for dynamical systems. *BMC Systems Biology*, 11(1):1–18, 2017.
- [5] Saifuddin Syed, Alexandre Bouchard-Côté, George Deligiannidis, and Arnaud Doucet. Non-reversible parallel tempering: a scalable highly parallel MCMC scheme. *Journal of the Royal Statistical Society: Series B*, 84:321–350, 2021.
- [6] Geneviève Lefebvre, Russell Steele, Alain C. Vandal, Sridar Narayanan, and Douglas L. Arnold. Path sampling to compute integrated likelihoods: an adaptive approach. *Journal of Computational and Graphical Statistics*, 18(2):415–437, 2009.
- [7] Geneviève Lefebvre, Russell Steele, and Alain C. Vandal. A path sampling identity for computing the Kullback–Leibler and J-divergences. *Computational Statistics & Data Analysis*, 54(7):1719–1731, 2010.
- [8] Silia Vitoratou and Ioannis Ntzoufras. Thermodynamic Bayesian model comparison. *Statistics and Computing*, 27(5):1165–1180, 2017.
- [9] Iwona Hawryluk, Swapnil Mishra, Seth Flaxman, Samir Bhatt, and Thomas A. Mellan. Referenced thermodynamic integration for Bayesian model selection: application to COVID-19 model selection. *arXiv:2009.03851*, 2021.
- [10] Ulrich Paquet, Ole Winther, and Manfred Opper. Perturbation Corrections in Approximate Inference: Mixture Modelling Applications. *Journal of Machine Learning Research*, 10(43):1263–1304, 2009.
- [11] Ewan Cameron and Anthony Pettitt. Recursive pathways to marginal likelihood estimation with prior-sensitivity analysis. *Statistical Science*, 29(3):397–419, 2014.
- [12] Jeremy Heng, Arnaud Doucet, and Yvo Pokern. Gibbs flow for approximate transport with applications to Bayesian computation. *Journal of the Royal Statistical Society: Series B*, 83(1):156–187, 2021.
- [13] Nando de Freitas, Pedro Højen-Sørensen, Michael I Jordan, and Stuart Russell. Variational MCMC. In *Uncertainty in Artificial Intelligence*, pages 120–127, 2001.
- [14] Jørund Gåsemyr. On an adaptive version of the Metropolis-Hastings algorithm with independent proposal distribution. *Scandinavian Journal of Statistics*, 30(1):159–173, 2003.
- [15] Håvard Rue, Ingelin Steinsland, and Sveinung Erland. Approximating hidden Gaussian Markov random fields. *Journal of the Royal Statistical Society: Series B*, 66(4):877–892, 2004.
- [16] Florian Maire, Nial Friel, Antonietta Mira, and Adrian E. Raftery. Adaptive incremental mixture Markov chain Monte Carlo. *Journal of Computational and Graphical Statistics*, 28(4):790–805, 2019.
- [17] Christophe Andrieu and Éric Moulines. On the ergodicity properties of some adaptive MCMC algorithms. *The Annals of Applied Probability*, 16(3):1462–1505, 2006.
- [18] Shixiang Gu, Zoubin Ghahramani, and Richard Turner. Neural adaptive sequential Monte Carlo. In *Advances in Neural Information Processing Systems*, volume 28, 2015.
- [19] Tim Salimans, Diederik Kingma, and Max Welling. Markov chain Monte Carlo and variational inference: bridging the gap. In *International Conference on Machine Learning*, pages 1218–1226, 2015.
- [20] Daniel Levy, Matthew Hoffman, and Jascha Sohl-Dickstein. Generalizing Hamiltonian Monte Carlo with neural networks. In *International Conference on Learning Representations*, 2018.
- [21] Matthew Hoffman. Learning deep latent Gaussian models with Markov Chain Monte Carlo. In *International Conference on Machine Learning*, pages 1510–1519, 2017.
- [22] Francisco Ruiz and Michalis Titsias. A contrastive divergence for combining variational inference and MCMC. In *International Conference on Machine Learning*, pages 5537–5545, 2019.
- [23] Jeffrey W Miller. Asymptotic normality, concentration, and coverage of generalized posteriors. *Journal of Machine Learning Research*, 22(168):1–53, 2021.

- [24] Ralf Herbrich. Minimising the Kullback-Leibler divergence. Technical report, Microsoft Research, 2005.
- [25] Jianqing Fan, Bai Jiang, and Qiang Sun. Hoeffding’s inequality for general Markov chains and its applications to statistical learning. *Journal of Machine Learning Research*, 22(139):1–35, 2021.
- [26] Alexandre Bouchard-Côté, Kevin Chern, Davor Cubranic, Sahand Hosseini, Justin Hume, Matteo Lepur, Zihui Ouyang, and Giorgio Sgarbi. Blang: Probabilistic Programming for Combinatorial Spaces. *Journal of Statistical Software*, 103:1–98, 2022.
- [27] Christian A. Naeseth, Fredrik Lindsten, and David Blei. Markovian score climbing: variational inference with KL(p||q). In *Advances in Neural Information Processing Systems*, pages 15499–15510, 2020.
- [28] Kyurae Kim, Jisu Oh, Jacob R. Gardner, Adji Bousso Dieng, and Hongseok Kim. Markov chain score ascent: A unifying framework of variational inference with Markovian gradients. In *Advances in Neural Information Processing Systems*, 2022.
- [29] Aad W van der Vaart. *Asymptotic Statistics*, volume 3. Cambridge University Press, 2000.
- [30] Olav Kallenberg. *Foundations of Modern Probability*. Springer, 2021.
- [31] Thomas A Severini. A comparison of the maximum likelihood estimator and the posterior mean in the single-parameter case. *Journal of the American Statistical Association*, 86(416): 997–1000, 1991.
- [32] Richard A Johnson. Asymptotic expansions associated with posterior distributions. *The Annals of Mathematical Statistics*, pages 851–864, 1970.
- [33] Anand G Dabak and Don H Johnson. Relations between Kullback-Leibler distance and Fisher information. 2002.
- [34] Guy Baele, Philippe Lemey, and Marc A. Suchard. Genealogical working distributions for Bayesian model testing with phylogenetic uncertainty. *Systematic Biology*, 65(2):250–264, 2016.
- [35] Michael Karcher, Cheng Zhang, and Frederick A. Matsen IV. Variational Bayesian supertrees. *arXiv:2104.11191*, 2021.
- [36] Radford M. Neal. Slice sampling. *The Annals of Statistics*, 31(3):705–767, 2003.
- [37] Saifuddin Syed, Vittorio Romaniello, Trevor Campbell, and Alexandre Bouchard-Côté. Parallel tempering on optimized paths. In *International Conference on Machine Learning*, volume 139, pages 10033–10042, 2021.
- [38] Błażej Miasojedow, Eric Moulines, and Matti Vihola. An adaptive parallel tempering algorithm. *Journal of Computational and Graphical Statistics*, 22(3):649–664, 2013.
- [39] Diederik P Kingma and Jimmy Ba. Adam: a method for stochastic optimization. In *International Conference on Learning Representations*, 2015.

Checklist

1. For all authors...
 - (a) Do the main claims made in the abstract and introduction accurately reflect the paper’s contributions and scope? **[Yes]** See the theoretical results (Section 3) and the experiments (Section 4).
 - (b) Did you describe the limitations of your work? **[Yes]** Limitations of the work are discussed in Section 3.5, where we assess the worst-case performance of the proposed method. We also note that chosen simulation examples are representative of various scenarios, including ones in which our method is comparable to a competitor.
 - (c) Did you discuss any potential negative societal impacts of your work? **[N/A]**
 - (d) Have you read the ethics review guidelines and ensured that your paper conforms to them? **[Yes]**
2. If you are including theoretical results...

- (a) Did you state the full set of assumptions of all theoretical results? [\[Yes\]](#) Theoretical assumptions are described and referenced in the theorem statements of Section 3. They are laid out in full in Appendix A and Appendix B.
 - (b) Did you include complete proofs of all theoretical results? [\[Yes\]](#) Complete proofs are provided in Appendices A-E.
3. If you ran experiments...
- (a) Did you include the code, data, and instructions needed to reproduce the main experimental results (either in the supplemental material or as a URL)? [\[Yes\]](#) We include our code in public GitHub repositories. These repositories also contain the data or instructions for obtaining the data.
 - (b) Did you specify all the training details (e.g., data splits, hyperparameters, how they were chosen)? [\[Yes\]](#) Experiments are described in detail in Appendix F.
 - (c) Did you report error bars (e.g., with respect to the random seed after running experiments multiple times)? [\[Yes\]](#) Instead of error bars, results of experiments that were repeated multiple times were displayed graphically to allow for approximate visual estimates of uncertainty. See, for example, Fig. 3.
 - (d) Did you include the total amount of compute and the type of resources used (e.g., type of GPUs, internal cluster, or cloud provider)? [\[Yes\]](#) The description of the resources used is provided in Appendix F.
4. If you are using existing assets (e.g., code, data, models) or curating/releasing new assets...
- (a) If your work uses existing assets, did you cite the creators? [\[Yes\]](#) See Appendix F for the list of models used and citations for the data sets.
 - (b) Did you mention the license of the assets? [\[Yes\]](#) Licenses are mentioned in Appendix F, which summarizes the models and data sets used.
 - (c) Did you include any new assets either in the supplemental material or as a URL? [\[Yes\]](#) We include our code in public GitHub repositories. These repositories also contain the data or instructions for obtaining the data.
 - (d) Did you discuss whether and how consent was obtained from people whose data you’re using/curating? [\[Yes\]](#) Licenses are described in Appendix F.
 - (e) Did you discuss whether the data you are using/curating contains personally identifiable information or offensive content? [\[N/A\]](#)
5. If you used crowdsourcing or conducted research with human subjects...
- (a) Did you include the full text of instructions given to participants and screenshots, if applicable? [\[N/A\]](#)
 - (b) Did you describe any potential participant risks, with links to Institutional Review Board (IRB) approvals, if applicable? [\[N/A\]](#)
 - (c) Did you include the estimated hourly wage paid to participants and the total amount spent on participant compensation? [\[N/A\]](#)

A PT-suitable reference family

Assumption A.1 (PT-suitable reference). *We say π_0 is PT-suitable for the target π_1 if:*

1. (Full support): $\text{supp}(\pi_0) = \text{supp}(\pi_1)$.
2. (Regularity): *The log-likelihood ratio between π_1 and π_0 , $\ell(x) = \log \frac{\pi_1(x)}{\pi_0(x)}$ satisfies,*

$$\max\{\mathbb{E}_0[|\ell|^3], \mathbb{E}_1[|\ell|^3]\} < \infty.$$

where we denote \mathbb{E}_0 , and \mathbb{E}_1 as the expectation with respect to π_0 and π_1 respectively.

We say that a family $\mathcal{Q} = \{q_\phi : \phi \in \Phi\}$ is PT-suitable for the target π_1 if for all ϕ the conditions above hold with q_ϕ in place of π_0 .

Assumption A.2 (Efficient local exploration). *Suppose π_0 is a PT-suitable reference for π_1 , with log-likelihood $\ell(x) = \log \pi_1(x) - \log \pi_0(x)$ and schedule \mathcal{B}_N . Let $\mathbf{X}_t = (X_t^0, \dots, X_t^N)$ be the PT chain stationary with respect to*

$$\pi(\mathbf{x}) = \prod_{n=0}^N \pi_{\beta_n}(x^n)$$

and K_{β_n} be the π_{β_n} -stationary Markov kernel for the local exploration step. We will say \mathbf{X}_t efficiently explores locally if [5, Section 3.3],

1. Stationarity: $\mathbf{X}_0 \sim \pi$.
2. Efficient local exploration (ELE) : *For all n and t , if $\bar{X}_t^n \sim K_{\beta_n}(X_t^n, d\bar{x})$, then $\ell(X_t^n)$ is independent of $\ell(\bar{X}_t^n)$.*

B Large-data Asymptotics

B.1 Conditional convergence in distribution

Suppose $(\mathcal{X}, d_{\mathcal{X}})$ is a metric space and let X, X_1, X_2, \dots be random variables taking values in \mathcal{X} . Define a sequence of σ -algebras $(\mathcal{F}_m)_{m=1}^\infty$ such that $\mathcal{F}_m \subset \mathcal{F}_{m+1}$. As $m \rightarrow \infty$, we say $X_m | \mathcal{F}_m$ converges in distribution to X , denoted $X_m | \mathcal{F}_m \xrightarrow{d} X$, if for all bounded and continuous $f : \mathcal{X} \rightarrow \mathbb{R}$,

$$\mathbb{E}[f(X_m) | \mathcal{F}_m] \xrightarrow[m \rightarrow \infty]{a.s.} \mathbb{E}[f(X)].$$

Similarly, we define conditional convergence in probability, denoted $X_m | \mathcal{F}_m \xrightarrow{p} X$, if for all $\epsilon > 0$,

$$\mathbb{P}(d_{\mathcal{X}}(X_m, X) > \epsilon | \mathcal{F}_m) \xrightarrow[m \rightarrow \infty]{a.s.} 0.$$

Lemma B.1 (Conditional portmanteau lemma). *The following are equivalent:*

1. $X_m | \mathcal{F}_m \xrightarrow{d} X$ as $m \rightarrow \infty$.
2. $\mathbb{E}[f(X_m) | \mathcal{F}_m] \xrightarrow{a.s.} \mathbb{E}[f(X)]$ as $m \rightarrow \infty$, for all bounded Lipschitz functions $f : \mathcal{X} \rightarrow \mathbb{R}$.
3. $\mathbb{P}[X_m \in A | \mathcal{F}_m] \xrightarrow{a.s.} \mathbb{P}[X \in A]$ as $m \rightarrow \infty$ for all $A \subset \mathcal{X}$ such that $\mathbb{P}[X \in \partial A] = 0$.

The proof of this Lemma is identical to the portmanteau lemma for weak convergence by replacing probabilities/expectations with conditional probabilities/expectations (for example, see [29, Section 2.1]).

Lemma B.2. *Suppose X, X_1, X_2, \dots and X', X_1, X_2, \dots are \mathcal{X} -valued random variables. Then, the following hold:*

1. If $X_m | \mathcal{F}_m \xrightarrow{d} X$ as $m \rightarrow \infty$ then $X_m \xrightarrow{d} X$.

2. If $X_m|\mathcal{F}_m \xrightarrow{p} X$ as $m \rightarrow \infty$ then $X_m \xrightarrow{p} X$.
3. If $X_m|\mathcal{F}_m \xrightarrow{p} X$ as $m \rightarrow \infty$ then $X_m|\mathcal{F}_m \xrightarrow{d} X$.
4. If $X_m|\mathcal{F}_m \xrightarrow{d} X$ as $m \rightarrow \infty$, and X is a constant a.s., then $X_m|\mathcal{F}_m \xrightarrow{p} X$.
5. Fatou's lemma: If $X_m|\mathcal{F}_m \xrightarrow{d} X$ as $m \rightarrow \infty$, then for all $f : \mathcal{X} \rightarrow [0, \infty)$,

$$\liminf_{m \rightarrow \infty} \mathbb{E}[f(X_m)|\mathcal{F}_m] \geq \mathbb{E}[f(X)], \quad a.s.$$
6. Continuous mapping theorem: If \mathcal{X}' is a metric space and $g : \mathcal{X} \rightarrow \mathcal{X}'$ is a continuous function, then

$$X_m|\mathcal{F}_m \xrightarrow[m \rightarrow \infty]{d} X \implies g(X_m)|\mathcal{F}_m \xrightarrow[m \rightarrow \infty]{d} g(X).$$

7. Slutsky's theorem: If $X_m|\mathcal{F}_m \xrightarrow{d} X$ and $d_{\mathcal{X}}(X'_m, X_m)|\mathcal{F}_m \xrightarrow{p} 0$, then $X'_m|\mathcal{F}_m \xrightarrow{d} X$.
8. Suppose $\mathcal{X} = \mathbb{R}^d$, with $X_m|\mathcal{F}_m \xrightarrow{d} X$. Suppose $A, A_1, \dots \in \mathbb{R}^{d \times d}$ such that $A, A_m \in \mathcal{F}_m$ and as $m \rightarrow \infty$ $A_m \xrightarrow{a.s.} A$, where A is a constant. Then,

$$A_m X_m|\mathcal{F}_m \xrightarrow[m \rightarrow \infty]{d} AX.$$

Proof of Lemma B.2.

1. For any bounded and continuous f ,

$$\lim_{m \rightarrow \infty} \mathbb{E}[f(X_m)] = \mathbb{E} \left[\lim_{m \rightarrow \infty} \mathbb{E}[f(X_m)|\mathcal{F}_m] \right] = \mathbb{E}[f(X)],$$

We can exchange the expectation and limit by the dominated convergence theorem.

2. For $\epsilon > 0$,

$$\mathbb{P}(d_{\mathcal{X}}(X_m, X) > \epsilon) = \mathbb{E}[\mathbb{P}(d_{\mathcal{X}}(X_m, X) > \epsilon|\mathcal{F}_m)]$$

Since $\mathbb{P}(d_{\mathcal{X}}(X_m, X) > \epsilon|\mathcal{F}_m) \xrightarrow{a.s.} 0$ as $m \rightarrow \infty$, the result follows from the dominated convergence theorem.

3. Let f be a κ -Lipschitz function bounded by M . Let $\epsilon > 0$,

$$\begin{aligned} |\mathbb{E}[f(X_m) - f(X)|\mathcal{F}_m]| &\leq \mathbb{E}[|f(X_m) - f(X)|1(d_{\mathcal{X}}(X_m, X) \leq \epsilon)|\mathcal{F}_m] \\ &\quad + \mathbb{E}[|f(X_m) - f(X)|1(d_{\mathcal{X}}(X_m, X) > \epsilon)|\mathcal{F}_m] \\ &= \kappa\epsilon + 2M\mathbb{P}(d_{\mathcal{X}}(X_m, X) > \epsilon|\mathcal{F}_m). \end{aligned}$$

Since $X_m \xrightarrow{p} X$ as $m \rightarrow \infty$, we have $\mathbb{P}(d_{\mathcal{X}}(X_m, X) > \epsilon|\mathcal{F}_m) \xrightarrow{a.s.} 0$, therefore

$$\lim_{m \rightarrow \infty} |\mathbb{E}[f(X_m) - f(X)|\mathcal{F}_m]| \leq \kappa\epsilon, \quad a.s.$$

The result follows by taking $\epsilon \rightarrow 0$.

4. Since X is a.s. constant there exists x_0 such that $\mathbb{P}(X = x_0) = 1$. Then for all $\epsilon > 0$, if $A_\epsilon = \{x : d_{\mathcal{X}}(x, x_0) > \epsilon\}$, we have $\mathbb{P}(X \in A_\epsilon) = 0$. Since $X_m|\mathcal{F}_m \xrightarrow{d} X$, we have

$$\mathbb{P}(d_{\mathcal{X}}(X_m, X) > \epsilon|\mathcal{F}_m) = \mathbb{P}(X_m \in A_\epsilon|\mathcal{F}_m) \xrightarrow[m \rightarrow \infty]{a.s.} \mathbb{P}(X \in A_\epsilon) = 0.$$

5. We adapt the proof of Fatou's lemma that holds for random variables that converge in distribution instead of almost surely adapted from [30, Lemma 5.11].

For any $K > 0$, we have $x \rightarrow x \wedge K$ is a bounded and continuous function. Since $X_m|\mathcal{F}_m \xrightarrow{d} X$, this implies that, almost surely,

$$\liminf_{m \rightarrow \infty} \mathbb{E}[X_m|\mathcal{F}_m] \geq \lim_{m \rightarrow \infty} \mathbb{E}[X_m \wedge K|\mathcal{F}_m] = \mathbb{E}[X \wedge K].$$

Since this is true for any K , and $X \wedge K \xrightarrow{a.s.} X$ as $K \rightarrow \infty$, by the monotone convergence theorem,

$$\liminf_{m \rightarrow \infty} \mathbb{E}[X_m | \mathcal{F}_m] \geq \lim_{K \rightarrow \infty} \mathbb{E}[X \wedge K] = \mathbb{E}[X].$$

6. Fix any bounded and continuous $f : \mathcal{X}' \rightarrow \mathbb{R}$. Because $f \circ g : \mathcal{X} \rightarrow \mathbb{R}$ is a bounded and continuous function, and $X_m | \mathcal{F}_m \xrightarrow{d} X$, we have,

$$\mathbb{E}[f(g(X_m)) | \mathcal{F}_m] \xrightarrow{a.s.} \mathbb{E}[f(g(X))].$$

7. Let f be a κ -Lipschitz function bounded by M . By triangle inequality,

$$|\mathbb{E}[f(X'_m) - f(X) | \mathcal{F}_m]| \leq \mathbb{E}[|f(X'_m) - f(X_m)| | \mathcal{F}_m] + |\mathbb{E}[f(X_m) - f(X) | \mathcal{F}_m]|.$$

Since $X_m \xrightarrow{d} X$, we have $\mathbb{E}[f(X_m) - f(X) | \mathcal{F}_m] \xrightarrow{a.s.} 0$. Also for all $\epsilon > 0$, let $A_{\epsilon, m} = \{d_{\mathcal{X}}(X_m, X'_m) \leq \epsilon\}$. Note that

$$\begin{aligned} \mathbb{E}[|f(X_m) - f(X'_m)| | \mathcal{F}_m] &= \kappa \mathbb{E}[|f(X_m) - f(X'_m)| \mathbb{1}(A_{\epsilon, m}) | \mathcal{F}_m] \\ &\quad + \mathbb{E}[|f(X_m) - f(X'_m)| \mathbb{1}(A_{\epsilon, m}^c) | \mathcal{F}_m] \\ &\leq \kappa \epsilon + 2M \mathbb{P}(A_{\epsilon, m}^c | \mathcal{F}_m) \end{aligned}$$

Since $d_{\mathcal{X}}(X_m, X'_m) | \mathcal{F}_m \xrightarrow{p} 0$, we have $\mathbb{P}(A_{\epsilon, m}^c | \mathcal{F}_m) \xrightarrow{a.s.} 0$. Also since $X_m | \mathcal{F}_m \xrightarrow{d} X$, we have $\mathbb{E}[f(X_m) - f(X) | \mathcal{F}_m] \xrightarrow{a.s.} 0$.

8. Fix $\epsilon > 0$. Note that

$$\begin{aligned} P(\|A_m - A\| > \epsilon | \mathcal{F}_m) &= \mathbb{E}[\mathbb{1}(\|A_m - A\| > \epsilon) | \mathcal{F}_m] \\ &= \mathbb{1}(\|A_m - A\| > \epsilon) \\ &\rightarrow 0 \quad a.s. \end{aligned}$$

This implies $A_m | \mathcal{F}_m \xrightarrow{p} A$ as $m \rightarrow \infty$.

Note that $(X_m, A) | \mathcal{F}_m \xrightarrow{d} (X, A)$ by the continuous mapping theorem with $x \rightarrow (x, A)$. Next, note that $\|(X_m, A_m) - (X_m, A)\| = \|A_m - A\|$, where use the matrix element-wise Euclidean norm. We are given that $A_m | \mathcal{F}_m \xrightarrow{p} A$. We now show that $(X_m, A_m) | \mathcal{F}_m \xrightarrow{d} (X, A)$. To this end, note that

$$(X_m, A) | \mathcal{F}_m \xrightarrow{d} (X, A), \quad (0, A_m) | \mathcal{F}_m \xrightarrow{p} (0, A).$$

Because $\|(X_m, A_m) - (X_m, A)\| = \|(0, A_m - A)\| = \|A_m - A\|$ and $A_m | \mathcal{F}_m \xrightarrow{p} A$, we have by Slutsky's theorem $(X_m, A_m) | \mathcal{F}_m \xrightarrow{d} (X, A)$. The result follows by an application of the continuous mapping theorem with the function $(x, A) \rightarrow Ax$. □

B.2 Model assumptions

The following sets of assumptions are only used to prove the large-data limit results of Proposition 3.1, Proposition 3.2, and Proposition 3.3. We suppose the data is $\mathbf{Y}_m = \{Y_i\}_{i=1}^m$ drawn i.i.d. from distribution $L(y; x_0) dy$, where $L(y; x)$ defines a statistical model parametrized by $x \in \mathcal{X}$ where \mathcal{X} is an open subset of \mathbb{R}^d . We denote the log-likelihood function ℓ and ℓ_m for the model and data respectively as,

$$\ell(y; x) = \log L(y; x), \quad \ell_m(x) = \sum_{i=1}^m \ell(Y_i; x)$$

We denote $x_{\text{MLE}, m}$ to be the maximum likelihood estimator

$$x_{\text{MLE}, m} \in \arg \max_x \ell_m(x).$$

We will use ℓ' and ℓ'' to denote the gradient and Hessian of ℓ with respect to x , and use $I(x)$ to denote the Fisher information matrix,

$$I(x) = -\mathbb{E}[\ell''(Y; x)] = -\int \ell''(y; x)L(y; x)dy,$$

and $I_m(x)$ for the observed information,

$$I_m(x) = -\ell''_m(x) = -\sum_{i=1}^m \ell''(Y_i; x).$$

We will always use a subscript m to indicate that the quantity is dependent on the data.

Given a prior π_0 distribution over \mathcal{X} , we define the posterior, $\pi_{1,m}$ with density conditional on \mathbf{Y}_m ,

$$\pi_{1,m}(x) \propto \pi_0(x) \prod_{i=1}^m L(Y_i; x) = \pi_0(x) \exp(\ell_m(x)).$$

We will use $\pi_{\beta,m}$ to denote the power posterior

$$\pi_{\beta,m} \propto \pi_0(x) \exp(\beta \ell_m(x)).$$

For the remainder of this section we will assume the following regularity conditions.

Assumption B.3.

1. *Euclidean state space:* $\mathcal{X} \subset \mathbb{R}^d$ has an open set containing x_0 .
2. *Continuity of prior density:* The prior density π_0 is continuous and positive in a neighbourhood of x_0 .
3. *Regularity of log-likelihood:* There is $K > 0$, such that for $\|x - x_0\| \leq K$, $\ell(y; x)$ continuously 3 times differentiable, and there is a $M(y)$ such that,

$$|\ell'''(y; x)| \leq M(y), \quad \int M(y)L(y; x_0)dy < \infty.$$

4. *Score at the MLE:* For all m , $x_{\text{MLE},m}$ exists, is unique, and $\ell'_m(x_{\text{MLE},m}) = 0$ almost surely.
5. *Strong consistency of MLE:* $x_{\text{MLE},m} \xrightarrow{a.s.} x_0$ as $m \rightarrow \infty$.
6. *Fisher information:* $I(x)$ is positive definite and continuous on a neighbourhood of x_0 .
7. *PT-Suitable:* For all m , both π_0 and \mathcal{Q} are almost surely PT-suitable for the posterior $\pi_{1,m}$ (see Assumption A.1).
8. *Efficient local exploration:* For all m , the PT chain with target $\pi_{1,m}$ and references in $\{\pi_0\} \cup \mathcal{Q}$, efficiently explore locally almost surely (see Assumption A.2).
9. *Bernstein-von Mises:* For $0 < \beta \leq 1$ and $X_{\beta,m} \sim \pi_{\beta,m}$ and $\mathbf{Y}_m \stackrel{iid}{\sim} L(\cdot; x_0)$,

$$m^{1/2}(X_{\beta,m} - x_{\text{MLE},m}) | \mathbf{Y}_m \xrightarrow{d} Z,$$

where $Z = N(0, \beta^{-1}I(x_0)^{-1})$.

Note that Assumption B.3.9 at $\beta = 1$ can be satisfied by introducing appropriate regularity conditions. See the paper ‘‘Asymptotic Normality, Concentration, and Coverage of Generalized Posteriors’’ by Miller (2021) for some possible conditions. For $0 < \beta < 1$, the result for the power posterior holds by noting that the tempered log-likelihood is $\beta \cdot \ell$ and by invoking Bernstein-von Mises results on the tempered log-likelihood under model misspecification (where the true data generating mechanism is based on the non-tempered likelihood). Such results for model misspecification are also available in the mentioned paper.

B.3 Preliminary results

We start off with an expansion of the log-likelihood, ℓ , about the MLE, $x_{\text{MLE},m}$. Define

$$Q_m(x) = -\frac{1}{2} \cdot (x - x_{\text{MLE},m})^\top I_m(x_{\text{MLE},m})(x - x_{\text{MLE},m}).$$

We bound the difference between the log-likelihood at the MLE and the second-order term in the expansion of the log-likelihood.

Lemma B.4. *Suppose Assumption B.3 holds. Then,*

1. $m^{-1}I_m(x_{\text{MLE},m}) \xrightarrow{\text{a.s.}} I(x_0)$ as $m \rightarrow \infty$.
2. For all $\|x - x_0\| < K/2$, we have a.s. there is an \bar{m} large enough such that for $m \geq \bar{m}$

$$\ell_m(x) = \ell_m(x_{\text{MLE},m}) + Q_m(x) + \epsilon_m(x)$$

for some $\epsilon_m(x)$ satisfying

$$|\epsilon_m(x)| \leq \frac{Mm}{3} \cdot \|x - x_{\text{MLE},m}\|^3,$$

and $M = \int M(y)L(y; x_0)dy < \infty$.

3. For any sequence of random variables, X_m , such that $m^{1/2}(X_m - x_{\text{MLE},m})|\mathbf{Y}_m \xrightarrow{d} X$ for some random variable X , we have

$$\begin{aligned} \epsilon_m(X_m)|\mathbf{Y}_m &\xrightarrow{p} 0, \\ \pi_0(X_m)|\mathbf{Y}_m &\xrightarrow{p} \pi_0(x_0). \end{aligned}$$

Proof of Lemma B.4. 1. By the triangle inequality,

$$\begin{aligned} \|m^{-1}I_m(x_{\text{MLE},m}) - I(x_0)\| &\leq \|m^{-1}I_m(x_{\text{MLE},m}) - m^{-1}I_m(x_0)\| \\ &\quad + \|m^{-1}I_m(x_0) - I(x_0)\|. \end{aligned}$$

We will now show that each term converges to 0 a.s.

Since $x_{\text{MLE},m} \xrightarrow{\text{a.s.}} x_0$, we have a.s., for m large enough $\|x_0 - x_{\text{MLE},m}\| < K$. Therefore by the mean-value theorem,

$$\begin{aligned} \|m^{-1}I_m(x_{\text{MLE},m}) - m^{-1}I_m(x_0)\| &= \frac{1}{m} \sum_{i=1}^m \|\ell''(Y_i; x_{\text{MLE},m}) - \ell''(Y_i; x_0)\| \\ &\leq \frac{1}{m} \sum_{i=1}^m M(Y_i) \|x_{\text{MLE},m} - x_0\|. \end{aligned}$$

Since $x_{\text{MLE},m} \xrightarrow{\text{a.s.}} x_0$, and $\frac{1}{m} \sum_{i=1}^m M(Y_i) \xrightarrow{\text{a.s.}} \int M(Y)L(y; x_0)dy < \infty$, we have

$$\|m^{-1}I_m(x_{\text{MLE},m}) - m^{-1}I_m(x_0)\| \xrightarrow[m \rightarrow \infty]{\text{a.s.}} 0.$$

By the strong law of large numbers we have

$$m^{-1}I_m(x_0) = \frac{1}{m} \sum_{i=1}^m \ell''(Y_i; x_0) \xrightarrow[m \rightarrow \infty]{\text{a.s.}} \int \ell''(y; x_0)L(y; x_0)dy = I(x_0).$$

This implies

$$\|m^{-1}I_m(x_0) - I(x_0)\| \xrightarrow[m \rightarrow \infty]{\text{a.s.}} 0.$$

2. We use a second-order expansion around $x_{\text{MLE},m}$ and Assumption B.3.4 to get,

$$\begin{aligned}\ell_m(x) &= \ell_m(x_{\text{MLE},m}) + (x - x_{\text{MLE},m})^\top \ell'_m(x_{\text{MLE},m}) + Q_m(x) + \epsilon_m(x) \\ &= \ell_m(x_{\text{MLE},m}) + Q_m(x) + \epsilon_m(x),\end{aligned}$$

for some $\epsilon_m(x)$ satisfying,

$$|\epsilon_m(x)| \leq \frac{M_m}{6} \|x - x_{\text{MLE},m}\|^3.$$

where $M_m = \sup\{|\ell'''_m(\xi)| : \|\xi - x_{\text{MLE},m}\| < \|x - x_{\text{MLE},m}\|\}$. We are done if we can show that $M_m \leq 2Mm$.

Suppose $\|\xi - x_{\text{MLE},m}\| < \|x - x_{\text{MLE},m}\|$. Then, by triangle inequality,

$$\begin{aligned}\|\xi - x_0\| &\leq \|\xi - x_{\text{MLE},m}\| + \|x_{\text{MLE},m} - x_0\| \\ &\leq \|x - x_{\text{MLE},m}\| + \|x_{\text{MLE},m} - x_0\| \\ &\leq \|x - x_0\| + \|x_0 - x_{\text{MLE},m}\| + \|x_{\text{MLE},m} - x_0\| \\ &< \frac{K}{2} + 2\|x_0 - x_{\text{MLE},m}\|\end{aligned}$$

By the strong consistency of the MLE Assumption B.3.5, we have a.s. there is an m_0 large enough such that for $m \geq m_0$, $\|x_{\text{MLE},m} - x_0\| < K/4$ and thus $\|\xi - x_0\| < K$. This means that Assumption B.3.3 implies,

$$|\ell'''_m(\xi)| \leq \sum_{i=1}^m |\ell'''(Y_i; \xi)| \leq \sum_{i=1}^m M(Y_i).$$

Since $Y_i \sim L(y; x_0)dy$, the law of large numbers implies $m^{-1} \sum_{i=1}^m M(Y_i)$ converges a.s. to M as $m \rightarrow \infty$. Almost surely, there is an $\bar{m} \geq m_0$ such that for $m \geq \bar{m}$,

$$\frac{1}{m} \sum_{i=1}^m M(Y_i) < 2M < \infty.$$

Therefore, $M_m \leq 2mM$, which completes the proof.

3. Note that $\epsilon_m(X_m)$ satisfies almost surely for m large enough,

$$|\epsilon_m(X_m)| \leq \frac{M}{3m^{1/2}} \|m^{1/2}(X_m - x_{\text{MLE},m})\|^3.$$

By the conditional continuous mapping theorem, Lemma B.2.6,

$$\|m^{1/2}(X_m - x_{\text{MLE},m})\|^3 | \mathbf{Y}_m \xrightarrow{d} \|X\|^3,$$

and $\epsilon_m(X_m) | \mathbf{Y}_m \xrightarrow{d} 0$ and hence also $\epsilon_m(X_m) | \mathbf{Y}_m \xrightarrow{p} 0$ and $\epsilon_m(X_m) \xrightarrow{p} 0$ by Lemma B.2.4.

Also note that $m^{1/2}(X_m - x_{\text{MLE},m}) | \mathbf{Y}_m \xrightarrow{d} X$ implies $X_m - x_{\text{MLE},m} | \mathbf{Y}_m \xrightarrow{p} 0$, and hence by the continuous mapping theorem, $\pi_0(X_m) | \mathbf{Y}_m \xrightarrow{p} \pi_0(x_0)$. □

Next, we claim that the second-order term in the expansion of the log-likelihood around the MLE evaluated at an appropriate random variable converges to a transformed chi-squared random variable. This result will be used repeatedly in the proofs of Proposition 3.1, Proposition 3.2, and Proposition 3.3.

Lemma B.5. *Suppose Assumption B.3 holds. If $X_{\beta,m}, X'_{\beta,m} \sim \pi_{\beta,m}$, are independent conditioned on \mathbf{Y}_m , then for all $0 < \beta \leq 1$ we have as $m \rightarrow \infty$:*

1. $\epsilon_m(X_{\beta,m}) | \mathbf{Y}_m \xrightarrow{p} 0$.
2. $Q_m(X_{\beta,m}) | \mathbf{Y}_m \xrightarrow{d} -Q/(2\beta)$, where $Q \sim \chi_d^2$.

3. $Q_m(X_{\beta,m}) - Q_m(X'_{\beta,m}) | \mathbf{Y}_m \xrightarrow{d} \frac{1}{2\beta}(Q - Q')$, where $Q, Q' \stackrel{iid}{\sim} \chi_d^2$.
4. $\ell_m(X_{\beta,m}) - \ell_m(X'_{\beta,m}) | \mathbf{Y}_m \xrightarrow{d} \frac{1}{2\beta}(Q - Q')$, where $Q, Q' \stackrel{iid}{\sim} \chi_d^2$.

Proof of Lemma B.5. 1. This follows immediately Assumption B.3.9. and Lemma B.4.3.

2. Note that we can decompose Q_m as

$$Q_m(X_{\beta,m}) = -\frac{1}{2}[m^{1/2}(X_{\beta,m} - x_{\text{MLE},m})]^\top \left[\frac{1}{m} I_m(x_{\text{MLE},m}) \right] [m^{1/2}(X_{\beta,m} - x_{\text{MLE},m})].$$

By Assumption B.3.9 we have,

$$m^{1/2}(X_{\beta,m} - x_{\text{MLE},m}) | \mathbf{Y}_m \xrightarrow[m \rightarrow \infty]{d} N(0, \beta^{-1} I^{-1}(x_0)),$$

and $m^{-1} I_m(x_{\text{MLE},m}) \xrightarrow{a.s.} I(x_0)$ by Assumption B.3.6. By Lemma B.2.7 and B.2.6 we get,

$$Q_m(X_{\beta,m}) | \mathbf{Y}_m \xrightarrow[m \rightarrow \infty]{d} -Q/(2\beta),$$

where $Q \sim \chi_d^2$.

3. Note that for any $0 < \beta \leq 1$, by using the arguments as above,

$$Q_m(X_{\beta,m}) | \mathbf{Y}_m \xrightarrow{d} -Q/(2\beta)$$

$$Q_m(X'_{\beta,m}) | \mathbf{Y}_m \xrightarrow{d} -Q/(2\beta),$$

where $Q \sim \chi_d^2$. Each of the $X_{\beta,m}, X'_{\beta,m}$ are assumed to be conditionally independent given the data \mathbf{Y}_m , and therefore

$$Q_m(X_{\beta,m}) - Q_m(X'_{\beta,m}) | \mathbf{Y}_m \xrightarrow[m \rightarrow \infty]{d} (Q - Q')/(2\beta),$$

where $Q, Q' \sim \chi_d^2$ are independent.

4. Finally, we employ Lemma B.4.2 and triangle inequality to get,

$$|[\ell_m(X_{\beta,m}) - \ell_m(X'_{\beta,m})] - [Q_m(X_{\beta,m}) - Q_m(X'_{\beta,m})]| \leq |\epsilon_m(X_{\beta,m})| + |\epsilon_m(X'_{\beta,m})|$$

By part Lemma B.5.1, we have $\epsilon_m(X_{\beta,m}) | \mathbf{Y}_m \xrightarrow{p} 0$ and $\epsilon_m(X'_{\beta,m}) | \mathbf{Y}_m \xrightarrow{p} 0$ so

$$[\ell_m(X_{\beta,m}) - \ell_m(X'_{\beta,m})] - [Q_m(X_{\beta,m}) - Q_m(X'_{\beta,m})] | \mathbf{Y}_m \xrightarrow{p} 0.$$

By Lemma B.5.3 and the conditional Slutsky's theorem Lemma B.2.7,

$$\ell_m(X_{\beta,m}) - \ell_m(X'_{\beta,m}) | \mathbf{Y}_m \xrightarrow[m \rightarrow \infty]{d} (Q - Q')/(2\beta).$$

□

B.4 Proof of Proposition 3.1

Proof of Proposition 3.1. The asymptotic restart rate, τ_m , is related to the GCB by

$$\tau_m = \frac{1}{2 + 2\Lambda(\pi_0, \pi_{1,m})},$$

where $\Lambda(\pi_0, \pi_{1,m})$ is the GCB between the prior π_0 and the posterior $\pi_{1,m}$. This implies that

$$0 \leq \limsup_{m \rightarrow \infty} \tau_m \leq \frac{1}{2 + 2 \liminf_{m \rightarrow \infty} \Lambda(\pi_0, \pi_{1,m})}.$$

Therefore, we are done if we can show that $\liminf_{m \rightarrow \infty} \Lambda(\pi_0, \pi_{1,m}) = \infty$ almost surely.

Suppose $X_{\beta,m}, X'_{\beta,m} \sim \pi_{\beta,m}$ are independent conditioned on \mathbf{Y}_m . Then,

$$\Lambda(\pi_0, \pi_{1,m}) = \frac{1}{2} \int_0^1 \mathbb{E}[\ell_m(X_{\beta,m}) - \ell(X'_{\beta,m}) | \mathbf{Y}_m] d\beta.$$

Since the integrand is positive, for any $\delta > 0$,

$$\Lambda(\pi_0, \pi_{1,m}) \geq \frac{1}{2} \int_\delta^1 \mathbb{E}[\ell_m(X_{\beta,m}) - \ell(X'_{\beta,m}) | \mathbf{Y}_m] d\beta$$

By taking the limit infimum of both sides, and using Fatou's lemma,

$$\liminf_{m \rightarrow \infty} \Lambda(\pi_0, \pi_{1,m}) \geq \frac{1}{2} \int_\delta^1 \liminf_{m \rightarrow \infty} \mathbb{E}[\ell_m(X_{\beta,m}) - \ell(X'_{\beta,m}) | \mathbf{Y}_m] d\beta.$$

From Lemma B.5.4 and the conditional continuous mapping theorem Lemma B.2.6 applied to $x \rightarrow |x|$, we have

$$|\ell_m(X_{\beta,m}) - \ell(X'_{\beta,m})| | \mathbf{Y}_m \xrightarrow[m \rightarrow \infty]{d} \frac{|Q - Q'|}{2\beta}, \quad Q, Q' \sim \chi_d^2.$$

By Lemma B.2.5, almost surely we have

$$\liminf_{m \rightarrow \infty} \Lambda(\pi_0, \pi_{1,m}) \geq \frac{1}{2} \int_\delta^1 \frac{1}{2\beta} \mathbb{E}[|Q - Q'|] d\beta = -\frac{1}{4} \mathbb{E}[|Q - Q'|] \log(\delta).$$

Since this is true for all $\delta > 0$, and since the right hand side increases to infinity as $\delta \rightarrow 0$, we have almost surely,

$$\liminf_{m \rightarrow \infty} \Lambda(\pi_0, \pi_{1,m}) \geq \lim_{\delta \rightarrow 0} -\frac{1}{4} \mathbb{E}[|Q - Q'|] \log(\delta) = \infty.$$

□

B.5 Proof of Proposition 3.2

Lemma B.6. Assume π_0 is a PT-suitable reference for π_1 , with log-likelihood ℓ .

1. If $L_\beta = \ell(X_\beta)$, for $X_\beta \sim \pi_\beta$, then L_β is stochastically non-decreasing in β , i.e. for all $y \in \mathbb{R}$, $\mathbb{P}(L_\beta > y)$ is a non-decreasing function of β .
2. Let $r(\beta, \beta')$ be a mean rejection rate for a swap between $\pi_\beta, \pi_{\beta'}$,

$$r(\beta, \beta') = 1 - \mathbb{E} \left[1 \wedge \frac{\pi_\beta(X_{\beta'}) \pi_{\beta'}(X_\beta)}{\pi_\beta(X_\beta) \pi_{\beta'}(X_{\beta'})} \right], \quad (X_\beta, X_{\beta'}) \sim \pi_\beta \times \pi_{\beta'}.$$

If $[a, b] \subset [a', b'] \subset [0, 1]$, then $r(a, b) \leq r(a', b')$.

Proof of Lemma B.6. 1. Fix $y \in \mathbb{R}$, and $0 \leq \beta < \beta' \leq 1$. We want to show that

$$0 \leq \mathbb{P}[L_{\beta'} > y] - \mathbb{P}[L_\beta > y] = \mathbb{E}[f(L_\beta, L_{\beta'})],$$

where $f(l, l') = 1(l' > y) - 1(l > y)$. We have

$$\begin{aligned} \mathbb{E}[f(L_\beta, L_{\beta'})] &= \int f(\ell(x), \ell(x')) \frac{1}{Z(\beta)} \exp(\beta \ell(x)) \frac{1}{Z(\beta')} \exp(\beta' \ell(x')) dx dx' \\ &= \frac{Z(\beta)}{Z(\beta')} \mathbb{E}[f(L, L') \exp(\delta L)], \end{aligned}$$

where $L, L' \stackrel{d}{=} \ell(X_\beta)$ are independent and $\delta = \beta' - \beta > 0$. Now, notice that

$$\begin{aligned} f(l, l') &= 1(l' > y) - 1(l > y) \\ &= 1(l' > y)1(l \leq y) - 1(l > y)1(l' \leq y). \end{aligned}$$

Therefore, we have

$$\begin{aligned}\mathbb{E}[f(L, L') \exp(\delta L')] &= \mathbb{E}[1(L' > y)1(L \leq y) \exp(\delta L')] \\ &\quad - \mathbb{E}[1(L > y)1(L' \leq y) \exp(\delta L')] \\ &= \mathbb{E}[1(L' > y)1(L \leq y)(\exp(\delta L') - \exp(\delta L))] \\ &\geq 0,\end{aligned}$$

where the second to last line used the fact that L, L' are i.i.d.

2. To simplify notation, suppose first $a = a'$. Denote the cumulative distribution function of L_β by F_β . From (a), we have that $F_b \geq F_{b'}$. It follows that we can construct a random variable L' which is equal in distribution to $L_{b'}$ and such that $L_b(\omega) \leq L'(\omega)$ for all outcomes ω in the probability space. This is achieved by setting $L' = F_{L_{b'}}^{-1} \circ F_{L_b} \circ L_b$, where F^{-1} denotes the generalized inverse cumulative function. To see why, note that $F_{L_b} \circ L_b$ is uniformly distributed, being a probability integral transform. Hence $F_{L_{b'}}^{-1}$ applied to that uniform yields a $L_{b'}$ -distributed random variable. The inequality $L_b(\omega) \leq L'(\omega)$ follows from $F_b \geq F_{b'}$. Next, define $f(\delta) = 1 - 1 \wedge \exp(-\delta)$, which is an increasing function in δ . Hence, $f((b-a)(L_b - L_a)) \leq f((b-a)(L' - L_a))$ for all outcomes, and so

$$r(a, b) = \mathbb{E}[f((b-a)(L_b - L_a))] \leq \mathbb{E}[f((b-a)(L' - L_a))] = r(a, b'),$$

where in the last equality we also used that L' is independent of L_a , being a deterministic transformation of the random variable L_b . Finally, if $a < a'$, use $r(a, b) \leq r(a, b') \leq r(a', b')$ where the last inequality is obtained using a very similar argument as above. \square

Lemma B.7. *Suppose \mathcal{Q} is almost surely a PT-suitable reference family for all targets $\pi_{1,m}$. Also assume that for all m , the PT chain with target $\pi_{1,m}$ and references \mathcal{Q} , efficiently explore locally almost surely. Given a (random) sequence $q_m \in \mathcal{Q}$, if α_m is the average acceptance probability between q_m and $\pi_{1,m}$, then if $\alpha_m \xrightarrow{p} 1$, then for any \mathcal{B}_N , we have $\tau_m(\mathcal{B}_N) \xrightarrow{p} \frac{1}{2}$ as $m \rightarrow \infty$.*

Proof of Lemma B.7. For any schedule $\mathcal{B}_n = (\beta_n)_{n=0}^N$, let $\{r_{n,m}\}_{n=0}^{N-1}$ be the average rejection rates between components n and $n+1$. For any n , we have by Lemma B.6,

$$0 \leq r_{n,m} \leq 1 - \alpha_m.$$

Since $\alpha_m \xrightarrow{p} 1$, we have $r_{n,m} \xrightarrow{p} 0$ as $m \rightarrow \infty$ and

$$\tau_m(\mathcal{B}_N) = \frac{1}{2 + 2 \sum_{n=0}^{N-1} \frac{r_{n,m}}{1-r_{n,m}}} \xrightarrow{p, m \rightarrow \infty} 1/2.$$

\square

Lemma B.8. *Suppose Assumption B.3 holds and $X_{0,m} \sim N(x_{\text{MLE},m}, I_m(x_{\text{MLE},m})^{-1})$. Then, as $m \rightarrow \infty$,*

$$m^{1/2}(X_{0,m} - x_{\text{MLE},m}) | \mathbf{Y}_m \xrightarrow{d} \mathcal{N}(0, I^{-1}(x_0)).$$

Proof of Lemma B.8. Since $X_{0,m} \sim N(x_{\text{MLE},m}, I_m(x_{\text{MLE},m})^{-1})$,

$$m^{1/2} \cdot \frac{I_m^{1/2}(x_{\text{MLE},m})}{m^{1/2}} \cdot I^{-1/2}(x_0)(X_{0,m} - x_{\text{MLE},m}) | \mathbf{Y}_m \sim \mathcal{N}(0, I^{-1}(x_0)).$$

By Lemma B.4.1 and Assumption B.3.5, we have

$$\frac{I_m^{1/2}(x_{\text{MLE},m})}{m^{1/2}} \cdot I^{-1/2}(x_0) \xrightarrow{a.s., m \rightarrow \infty} \mathbb{I}_d.$$

By Lemma B.2.7 it follows,

$$m^{1/2}(X_{0,m} - x_{\text{MLE},m}) | \mathbf{Y}_m \xrightarrow{d} \mathcal{N}(0, I^{-1}(x_0)).$$

\square

Proof of Proposition 3.2. Let $q_m = N(x_{\text{MLE},m}, I_m^{-1}(x_{\text{MLE},m})) \in \mathcal{Q}$. The acceptance probability α_m is

$$\alpha_m = \mathbb{E}[1 \wedge A_m(X_{0,m}, X_{1,m}) | \mathbf{Y}_m],$$

where $A_m(X_{0,m}, X_{1,m})$ is the acceptance ratio,

$$\begin{aligned} A_m(X_{0,m}, X_{1,m}) &= \frac{q_m(X_{1,m}) \cdot \pi_{1,m}(X_{0,m})}{q_m(X_{0,m}) \cdot \pi_{1,m}(X_{1,m})} \\ &= \frac{q_m(X_{1,m})}{q_m(X_{0,m})} \cdot \frac{\pi_0(X_{0,m})}{\pi_0(X_{1,m})} \cdot \frac{\exp(\ell_m(X_{0,m}))}{\exp(\ell_m(X_{1,m}))}. \end{aligned}$$

Note that up to an additive constant $\log q_m(x) = Q_m(x)$, and so

$$\log q_m(X_{1,m}) - \log q_m(X_{0,m}) = Q_m(X_{1,m}) - Q_m(X_{0,m}).$$

Therefore the log-acceptance ratio satisfies

$$\log A_m(X_{0,m}, X_{1,m}) = \log \pi_0(X_{0,m}) - \log \pi_0(X_{1,m}) + \epsilon_m(X_{0,m}) - \epsilon_m(X_{1,m}),$$

where ϵ_m was defined in Lemma B.4.

Since we have the asymptotic normality of $X_{0,m}$ and $X_{1,m}$ conditioned on \mathbf{Y}_m by Lemma B.5.9, and Lemma B.8, we can invoke Lemma B.4.3,

$$\epsilon_m(X_{0,m}), \epsilon_m(X_{1,m}) | \mathbf{Y}_m \xrightarrow[m \rightarrow \infty]{p} 0, \quad (6)$$

$$\log \pi_0(X_{0,m}), \log \pi_0(X_{1,m}) | \mathbf{Y}_m \xrightarrow[m \rightarrow \infty]{p} \log \pi_0(x_0).$$

Combining (6) we have the acceptance ratio satisfies,

$$A_m(X_{0,m}, X_{1,m}) | \mathbf{Y}_m \xrightarrow{p} 1.$$

To conclude, note that $1 \wedge A_m(X_{0,m}, X_{1,m}) \leq 1$, so by the dominated convergence theorem,

$$\alpha_m = \mathbb{E}[1 \wedge A_m(X_{0,m}, X_{1,m}) | \mathbf{Y}_m] \xrightarrow[m \rightarrow \infty]{a.s.} 1,$$

and hence $\alpha_m \xrightarrow{a.s.} 1$. The result follows from Lemma B.7. \square

B.6 Proof of Proposition 3.3

Suppose μ_m and Σ_m are posterior mean and variance conditional to \mathbf{Y}_m ,

$$\mu_m = \mathbb{E}[X_{1,m} | \mathbf{Y}_m], \quad \Sigma_m = \text{Var}[X_{1,m} | \mathbf{Y}_m],$$

where $X_{1,m} \sim \pi_{1,m}$. We introduce a final set of assumptions that are required for the proof of Proposition 3.3.

Assumption B.9. 1. *Posterior mean and MLE:* As $m \rightarrow \infty$, $m^{1/2}(\mu_m - x_{\text{MLE},m}) \xrightarrow{a.s.} 0$.

2. *Posterior variance and Fisher information:* For all m , Σ_m is almost surely positive definite and $m\Sigma_m \xrightarrow{a.s.} I^{-1}(x_0)$ as $m \rightarrow \infty$.

For such results in the univariate case with convergence in probability, see [31] and [32].

Given $q'_m = N(\mu_m, \Sigma_m)$, define,

$$Q'_m(x) = -\frac{1}{2}(x - \mu_m)^\top \Sigma_m^{-1}(x - \mu_m).$$

Lemma B.10. *Suppose Assumption B.3 and Assumption B.9 hold. If $X'_{0,m} \sim q'_{0,m}$ and $X_{1,m} \sim \pi_{1,m}$, then as $m \rightarrow \infty$,*

1. $m^{1/2}(X'_{0,m} - x_{\text{MLE},m}) | \mathbf{Y}_m \xrightarrow{d} \mathcal{N}(0, I^{-1}(x_0))$,

2. $Q'_m(X_{1,m}) - Q_m(X_{1,m}) \xrightarrow{p} 0$,
3. $Q'_m(X'_{0,m}) - Q_m(X'_{0,m}) \xrightarrow{p} 0$.

Proof of Lemma B.10. 1. Note that since $X'_{0,m} \sim \mathcal{N}(\mu_m, \Sigma_m)$,

$$\frac{\Sigma_m^{-1/2}}{m^{1/2}} \cdot I^{-1/2}(x_0) \cdot m^{1/2}(X_{0,m} - \mu_m) | \mathbf{Y}_m \sim \mathcal{N}(0, I^{-1}(x_0)).$$

By Assumption B.9,

$$\frac{\Sigma_m^{-1/2}}{m^{1/2}} \cdot I^{-1/2}(x_0) \xrightarrow[m \rightarrow \infty]{a.s.} \mathbb{I}_d.$$

Therefore using Slutsky's theorem, Lemma B.2.7, it follows that

$$m^{1/2}(X'_{0,m} - \mu_m) | \mathbf{Y}_m \xrightarrow[m \rightarrow \infty]{d} \mathcal{N}(0, I^{-1}(x_0)).$$

Finally, the result follows from Slutsky's theorem using Assumption B.9.1.

2. Using the definition of $Q(x)$ and $Q'(x)$ we obtain the following decomposition,

$$Q'_m(x) - Q_m(x) = \epsilon_m^0 + \epsilon_m^1(x) + \epsilon_m^2(x)$$

where,

$$\begin{aligned} \epsilon_m^0 &= -(\mu_m - x_{\text{MLE},m})^\top \Sigma_m^{-1} (\mu_m - x_{\text{MLE},m}) \\ \epsilon_m^1(x) &= -2(x - x_{\text{MLE},m})^\top \Sigma_m^{-1} (x_{\text{MLE},m} - \mu_m) \\ \epsilon_m^2(x) &= -[m^{1/2}(x - x_{\text{MLE},m})]^\top \cdot [m^{-1}(\Sigma_m^{-1} - I_m(x_{\text{MLE},m}))] \cdot [m^{1/2}(x - x_{\text{MLE},m})] \end{aligned}$$

Now, using Assumption B.9, it follows that $\epsilon_m^0 \xrightarrow{p} 0$ as $m \rightarrow \infty$,

$$\begin{aligned} \epsilon_m^0 &= -[m^{1/2}(\mu_m - x_{\text{MLE},m})]^\top [m \Sigma_m]^{-1} [m^{1/2}(\mu_m - x_{\text{MLE},m})] \\ &= o_p(1) \cdot O_p(1) \cdot o_p(1) \\ &= o_p(1). \end{aligned}$$

Therefore we are done if we can show (1) $\epsilon_m^1(X_{1,m}) \xrightarrow{p} 0$ and (2) $\epsilon_m^2(X_{1,m}) \xrightarrow{p} 0$ as $m \rightarrow \infty$.

(1) follows from Assumption B.9 and Lemma B.5.9 since as $m \rightarrow \infty$,

$$\begin{aligned} \epsilon_m^1(X_{1,m}) &= -2[m^{1/2}(X_{1,m} - x_{\text{MLE},m})]^\top [m \Sigma_m]^{-1} [m^{1/2}(x_{\text{MLE},m} - \mu_m)] \\ &= O_p(1) \cdot O_p(1) \cdot o_p(1) \\ &= o_p(1). \end{aligned}$$

Finally for (2) notice that by Assumption B.9, and $m^{-1}(\Sigma_m^{-1} - I_m(x_{\text{MLE},m})) \xrightarrow{p} 0$. Using Lemma B.5.9 as $m \rightarrow \infty$,

$$\begin{aligned} \epsilon_m^2(X_{1,m}) &= -[m^{1/2}(X_{1,m} - x_{\text{MLE},m})]^\top [m^{-1}(\Sigma_m^{-1} - I_m(x_{\text{MLE},m}))] [m^{1/2}(X_{1,m} - x_{\text{MLE},m})] \\ &= O_p(1) \cdot o_p(1) \cdot O_p(1) \\ &= o_p(1) \end{aligned}$$

3. Similar to the proof of Lemma B.10.2, we are done if we can show (3) $\epsilon_m^1(X'_{0,m}) \xrightarrow{p} 0$ and (4) $\epsilon_m^2(X'_{0,m}) \xrightarrow{p} 0$ as $m \rightarrow \infty$.

To show (3) we use Lemma B.10.1 and Assumption B.9,

$$\begin{aligned} \epsilon_m^1(X'_{0,m}) &= -2[m^{1/2}(X'_{0,m} - x_{\text{MLE},m})]^\top [m \Sigma_m]^{-1} [m^{1/2}(x_{\text{MLE},m} - \mu_m)] \\ &= O_p(1) \cdot O_p(1) \cdot o_p(1) \\ &= o_p(1). \end{aligned}$$

Finally, to obtain (4) follows from Lemma B.10.1 and $m^{-1}(\Sigma_m^{-1} - I_m(x_{\text{MLE},m})) \xrightarrow{p} 0$,

$$\begin{aligned}\epsilon_m^2(X'_{0,m}) &= [m^{1/2}(X'_{0,m} - x_{\text{MLE},m})]^\top [m^{-1}(\Sigma_m^{-1} - I_m)] [m^{1/2}(X'_{0,m} - x_{\text{MLE},m})] \\ &= O_p(1) \cdot o_p(1) \cdot O_p(1) \\ &= o_p(1).\end{aligned}$$

□

Proof of Proposition 3.3. Suppose $X_{1,m} \sim \pi_{1,m}$ and $X'_{0,m} \sim q'_m = N(\mu_m, \Sigma_m) \in \mathcal{Q}$ are independent conditioned on \mathbf{Y}_m . Let $\alpha'_m = \mathbb{E}[1 \wedge A'_m(X'_{0,m}, X_{1,m})]$ be the average acceptance probability, where $A'_m(X'_{0,m}, X_{1,m})$ is the acceptance ratio,

$$\begin{aligned}A'_m(X'_{0,m}, X_{1,m}) &= \frac{q'_m(X_{1,m}) \cdot \pi_{1,m}(X'_{0,m})}{q'_m(X'_{0,m}) \cdot \pi_{1,m}(X_{1,m})} \\ &= \frac{q'_m(X_{1,m})}{q'_m(X'_{0,m})} \cdot \frac{\pi_0(X'_{0,m})}{\pi_0(X_{1,m})} \cdot \frac{\exp(\ell_m(X'_{0,m}))}{\exp(\ell_m(X_{1,m}))}.\end{aligned}$$

Note that up to an additive constant $\log q'_m(x) = Q'_m(x)$, and by Lemma B.10, we have as $m \rightarrow \infty$,

$$\begin{aligned}\log q'_m(X_{1,m}) - \log q'_m(X'_{0,m}) &= Q'_m(X_{1,m}) - Q'_m(X'_{0,m}), \\ &= Q_m(X_{1,m}) - Q_m(X'_{0,m}) + o_p(1).\end{aligned}$$

Therefore we have the log-acceptance ratio satisfies,

$$\log A'_m(X'_{0,m}, X_{1,m}) = \log \pi_0(X'_{0,m}) - \log \pi_0(X_{1,m}) + \epsilon_m(X'_{0,m}) - \epsilon_m(X_{1,m}) + o_p(1).$$

where ϵ_m was defined in Lemma B.4. By Lemma B.5.9, and Lemma B.10.1 we have $m^{1/2}(X_{1,m} - x_{\text{MLE},m})$ and $m^{1/2}(X'_{0,m} - x_{\text{MLE},m})$ are asymptotically normal conditioned on \mathbf{Y}_m . Therefore by Lemma B.4.3,

$$\begin{aligned}\epsilon_m(X'_{0,m}), \epsilon_m(X_{1,m}) &\xrightarrow{p, m \rightarrow \infty} 0 \\ \log \pi_0(X'_{0,m}), \log \pi_0(X_{1,m}) &\xrightarrow{p, m \rightarrow \infty} \log \pi_0(x_0),\end{aligned}$$

and the acceptance ratio $A'_m(X'_{0,m}, X_{1,m}) \xrightarrow{p} 1$.

To conclude, note that $1 \wedge A'_m(X'_{0,m}, X_{1,m}) \leq 1$, so by dominated convergence theorem,

$$\lim_{m \rightarrow \infty} \mathbb{E}[\alpha'_m] = \lim_{m \rightarrow \infty} \mathbb{E}[1 \wedge A'_m(X'_{0,m}, X_{1,m})] = 1,$$

and hence $\alpha'_m \xrightarrow{p} 1$.

□

C Proof of Theorem 3.4

Proof of Theorem 3.4. Since η is bounded there is a $K > 0$ such that $\eta(x) = (\eta_1(x), \dots, \eta_d(x))$ where $\eta_i : \mathcal{X} \rightarrow [-K, K]$. Fix $0 < \epsilon < \frac{1}{2}$. Suppose $(\mathbf{X}_{t,r})_{t=1}^{T_r}$ are the draws from the chain parameterized by $\hat{\phi}_r$ at round r . Define for each $i = 1, \dots, d$,

$$A_{r,i} = \left\{ \left| \frac{1}{T_r} \sum_{t=1}^{T_r} \eta_i(X_{t,r}^N) - \mathbb{E}_1[\eta_i] \right| > \delta_r \right\},$$

where δ_r is a sequence to be determined. By assumption, we have $|\eta_i(x)| \leq K$ for some $K > 0$. We can therefore apply Theorem 1 of [25] (Hoeffding's inequality for Markov chains) to get that

$$\begin{aligned} P(A_{r,i} | \hat{\phi}_r) &\leq 2 \exp \left(- \frac{\text{Gap}(\hat{\phi}_r)}{2 - \text{Gap}(\hat{\phi}_r)} \cdot \frac{\delta_r^2 T_r}{2K^2} \right) \\ &\leq 2 \exp \left(- \frac{\kappa}{2 - \kappa} \cdot \frac{\delta_r^2 T_r}{2K^2} \right). \end{aligned}$$

The last inequality used the assumption that $\text{Gap}(\phi)$ is bounded below by κ on Φ . By taking expectations over $\hat{\phi}_r$ and by setting $\delta_r = d^{-1} T_r^{-1/2+\epsilon}$, we obtain

$$P(A_{r,i}) \leq 2 \exp \left(- \frac{\kappa}{2 - \kappa} \cdot \frac{T_r^\epsilon}{2d^2 K^2} \right).$$

Since $T_r = \Omega(2^r)$, we have by the ratio test,

$$\sum_{r=1}^{\infty} P(A_{r,i}) < \infty.$$

From the Borel-Cantelli lemma it follows that for each i , $P(A_{r,i} \text{ i.o.}) = 0$, and thus a.s. there exists $R_i(\epsilon)$ and such that for all $r \geq R_i(\epsilon)$,

$$\left\| \frac{1}{T_r} \sum_{t=1}^{T_r} \eta_i(X_{t,r}^N) - \mathbb{E}_1[\eta_i] \right\| \leq \frac{1}{d} T_r^{-\frac{1}{2}+\epsilon}.$$

Since $\hat{\phi}_{r+1}$ is chosen to satisfy,

$$\mathbb{E}_{\hat{\phi}_{r+1}}[\eta] = \frac{1}{T_r} \sum_{t=1}^{T_r} \eta(X_{t,r}^N),$$

by the triangle inequality, we have for all $r > \max\{R_1(\epsilon), \dots, R_d(\epsilon)\} = R(\epsilon)$,

$$\|\mathbb{E}_{\hat{\phi}_{r+1}}[\eta] - \mathbb{E}_1[\eta]\| \leq T_r^{-\frac{1}{2}+\epsilon}$$

In particular, since $\mathbb{E}_1[\eta] = \mathbb{E}_{\phi_{\text{KL}}}[\eta]$, we have a.s.

$$\lim_{r \rightarrow \infty} \mathbb{E}_{\hat{\phi}_r}[\eta] = \mathbb{E}_{\phi_{\text{KL}}}[\eta].$$

Since \mathcal{Q} is an exponential family of full-rank, convergence in the mean of the sufficient statistic is equivalent to the convergence of the the natural parameters. That is,

$$\hat{\phi}_r \xrightarrow[r \rightarrow \infty]{a.s.} \phi_{\text{KL}}.$$

□

D Upper bounds on the GCB

D.1 Proof of Theorem 3.5

Suppose $X_{\phi,\beta}, X'_{\phi,\beta} \sim \pi_{\phi,\beta}$ are independent. By Jensen's inequality and Result 4 in [33],

$$\begin{aligned} \Lambda(q_\phi, \pi_1) &= \frac{1}{2} \int_0^1 \mathbb{E}[|\ell_\phi(X_{\phi,\beta}) - \ell_\phi(X'_{\phi,\beta})|] d\beta \\ &\leq \frac{1}{2} \left(\int_0^1 \mathbb{E}[(\ell_\phi(X_{\phi,\beta}) - \ell_\phi(X'_{\phi,\beta}))^2] d\beta \right)^{1/2} \\ &= \sqrt{\frac{1}{2} \text{SKL}(q_\phi, \pi_1)}. \end{aligned} \quad (7)$$

Also, because ϕ_{KL} minimizes the forward KL divergence, it follows that

$$\mathbb{E}_{\phi_{\text{KL}}}[\eta] = \mathbb{E}_{\pi_1}[\eta].$$

In particular, by taking a dot product with ϕ for any $\phi \in \Phi$ it holds that

$$\mathbb{E}_{\phi_{\text{KL}}}[\log q_\phi] - \mathbb{E}_{\pi_1}[\log q_\phi] = \mathbb{E}_{\phi_{\text{KL}}}[\log h] - \mathbb{E}_{\pi_1}[\log h]. \quad (8)$$

From Eq. (8),

$$\begin{aligned} |\text{SKL}(q_{\phi_{\text{KL}}}, \pi_1)| &= \left| \mathbb{E}_{\phi_{\text{KL}}} \left[\log \frac{\pi_1}{q_{\phi_{\text{KL}}}} \right] - \mathbb{E}_{\pi_1} \left[\log \frac{\pi_1}{q_{\phi_{\text{KL}}}} \right] \right| \\ &= \left| \mathbb{E}_{\phi_{\text{KL}}}[\log \pi_1] - \mathbb{E}_{\pi_1}[\log \pi_1] + \mathbb{E}_{\pi_1}[\log h] - \mathbb{E}_{\phi_{\text{KL}}}[\log h] \right| \\ &= \left| \mathbb{E}_{\phi_{\text{KL}}}[\log \pi_1 - \log q_{\phi_0}] - \mathbb{E}_{\pi_1}[\log \pi_1 - \log q_{\phi_0}] \right| \\ &\leq \mathbb{E}_{\phi_{\text{KL}}} [|\log \pi_1 - \log q_{\phi_0}|] + \mathbb{E}_{\pi_1} [|\log \pi_1 - \log q_{\phi_0}|] \\ &\leq \mathbb{E}_{\phi_{\text{KL}}}[g] + \mathbb{E}_{\pi_1}[g] \\ &\leq M_1 + M_2. \end{aligned} \quad (9)$$

Therefore, combining Eq. (7) and 9,

$$\Lambda(q_\phi, \pi_1) \leq \sqrt{\frac{1}{2}(M_1 + M_2)}.$$

D.2 Example with multivariate normal distributions

We consider here two simple examples to verify that the upper bound given by Theorem 3.5 is small enough for practical purposes.

To put into perspective the numerical values obtained in the examples below, note that the GCBs measured by [5] in 17 problems were in the range 0.4–88.

Example D.1. Suppose that $\pi_1 \sim N(0, \Sigma_1)$ and $q_\phi \sim N(0, \Sigma_0(\phi))$ where

$$\Sigma_1 = \begin{bmatrix} 1 & \rho \\ \rho & 1 \end{bmatrix} \quad \text{and} \quad \Sigma_0(\phi) = \begin{bmatrix} \phi_1 & 0 \\ 0 & \phi_2 \end{bmatrix}$$

for some $0 \leq \rho < 1$. By applying Theorem 3.5 we have

$$\Lambda(q_{\phi_{\text{KL}}}, \pi_1) \leq \sqrt{-\frac{1}{2} \log(1 - \rho^2) + \frac{\rho}{1 - \rho}}.$$

Substituting $\rho = 0.9, 0.95, 0.99$ provides GCB upper bounds of approximately 3.14, 4.49, 10.05, respectively, while we obtained values of $\Lambda(q_{\phi_{\text{KL}}}, \pi_1)$ of $\approx 0.8, 1.0$ and 1.5 using our stabilized moment matching algorithm. \triangleleft

Proof. Based on moment-matching, $\phi_{\text{KL}} = (1, 1)'$ and therefore $\Sigma_0(\phi_{\text{KL}}) = \mathbb{I}_2$ is the 2×2 identity matrix.

We have that

$$\begin{aligned}
|\log \pi_1(x) - \log q_{\phi_{\text{KL}}}(x)| &= \left| -\frac{1}{2} \log(1 - \rho^2) - \frac{1}{2} x^\top \Sigma_1^{-1} x + \frac{1}{2} x^\top \mathbb{I}_2 x \right| \\
&= \left| -\frac{1}{2} \log(1 - \rho^2) - \frac{1}{2} x^\top (\Sigma_1^{-1} - \mathbb{I}_2) x \right| \\
&\leq -\frac{1}{2} \log(1 - \rho^2) + \frac{1}{2} \|x\|^2 \max\{|\lambda_{\max}|, |\lambda_{\min}|\} \\
&= -\frac{1}{2} \log(1 - \rho^2) + \frac{1}{2} \|x\|^2 \max\left\{ \frac{\rho}{1 - \rho}, \frac{\rho}{1 + \rho} \right\} \\
&= -\frac{1}{2} \log(1 - \rho^2) + \frac{1}{2} \|x\|^2 \frac{\rho}{1 - \rho} \\
&=: g(x)
\end{aligned}$$

by the min-max eigenvalue theorem. It can then be verified that

$$M_1 = M_2 = -\frac{1}{2} \log(1 - \rho^2) + \frac{\rho}{1 - \rho}.$$

□

Example D.2. Suppose that the target is a mixture of normal distributions so that

$$\pi_1 \sim 0.5 \cdot N(-\mu, 1) + 0.5 \cdot N(\mu, 1) \quad \text{and} \quad q_\phi \sim N(0, \phi),$$

for some μ . We estimate the expectations in the upper bound of the GCB using Monte Carlo draws from $q_{\phi_{\text{KL}}}$ and π_1 . For $\mu = 5, 10, 100$ we find that $\Lambda(q_{\phi_{\text{KL}}}, \pi_1)$ is upper bounded by approximately 1.7, 3.2, and 32, respectively (up to Monte Carlo estimation error based on 1,000,000 Monte Carlo simulation draws for $\mu = 5, 10$, and 100,000,000 Monte Carlo simulations for $\mu = 100$), while we obtained values of $\Lambda(q_{\phi_{\text{KL}}}, \pi_1)$ of $\approx 2.3, 2.8$ and 4.2 using our stabilized moment matching algorithm. ◁

Proof. Based on moment-matching, we obtain that $\phi_{\text{KL}} = \mu^2 + 1$. Denote the pdf of the standard normal density by $\phi(\cdot)$. Then,

$$\begin{aligned}
|\log \pi_1(x) - \log q_{\text{KL}}(x)| &= \left| \log \left(\frac{1}{2} \phi(x + \mu) + \frac{1}{2} \phi(x - \mu) \right) - \frac{1}{\sqrt{\mu^2 + 1}} \cdot \phi \left(\frac{x}{\sqrt{\mu^2 + 1}} \right) \right| \\
&=: g(x).
\end{aligned}$$

□

E Proof of Theorem 3.6

The proof of this theorem is almost identical to the proof of Theorem 1 in [5]. The main difference is that we study two delayed renewal processes simultaneously instead of one.

First, define the index process for the j -th machine for $j = 0, 1, \dots, \bar{N}$ as $(n_t(j), \epsilon_t(j))$ where $n_t(j) \in \{0, 1, \dots, \bar{N}\}$, $\epsilon_t(j) \in \{-1, 1\}$, and $\bar{N} = N_\phi + N$. Here, $n_t(j)$ denotes the annealing parameter index for the j -th machine at iteration t and $\epsilon_t(j) = 1$ if after iteration t the annealing parameter on machine j will be proposed to increase to index $n_t(j) + 1$. Otherwise, $\epsilon_t(j) = -1$. In particular, machine j is storing annealing parameter $\bar{\beta}_{n_t(j)}$, and therefore $n_t(j) = 0, N_\phi, \bar{N}$ means the machine j is at the annealing parameter corresponding to q_ϕ, π_1, π_0 , respectively.

Informally, a restart occurs when a sample from *either* one of the two references reaches the target distribution chain. Because the target distribution is placed between the two references, we see that we can count the number of restarts by defining two delayed renewal processes and summing the number of restarts for each renewal process. We ensure that we are not double-counting any restarts by introducing two processes instead of one.

Machine j undergoes a restart from q_ϕ when $n_t(j)$ goes from 0 to N_ϕ . Similarly, we will say machine j undergoes a restart from π_0 when $n_t(j)$ goes from \bar{N} to N_ϕ . We define $\mathcal{T}_{\phi,t}(j)$ and $\mathcal{T}_t(j)$ to be the total number of restarts on machine j from q_ϕ and π_0 respectively by time iteration t . We will denote the total number of restarts by time t from q_ϕ and π_0 as $\mathcal{T}_{\phi,t}$ and \mathcal{T}_t respectively, so that

$$\mathcal{T}_{\phi,t} = \sum_{j=0}^{\bar{N}} \mathcal{T}_{\phi,t}(j), \quad \mathcal{T}_t = \sum_{j=0}^{\bar{N}} \mathcal{T}_t(j)$$

Formally, define

$$T_{\phi,0}^-(j) = \inf\{t : (n_t(j), \epsilon_t(j)) = (0, -1)\}$$

and then recursively define for $k \geq 1$

$$\begin{aligned} T_{\phi,k}^+(j) &= \inf\{t > T_{\phi,k-1}^-(j) : (n_t(j), \epsilon_t(j)) = (N_\phi, +1)\} \\ T_{\phi,k}^-(j) &= \inf\{n > T_{\phi,k}^+(j) : (n_t(j), \epsilon_t(j)) = (0, -1)\}. \end{aligned}$$

We note that $T_{\phi,k}^+(j)$ corresponds to the time of the k -th restart from q_ϕ on machine j and

$$\mathcal{T}_{\phi,t}(j) = \max\{k : T_{\phi,k}^+(j) \leq t\}.$$

We have $\mathcal{T}_{\phi,t}(j)$ is a delayed renewal process counting the number of times a sample travels from chain 0 (targeting q_ϕ) to chain N_1 (targeting π_1) with inter-arrival times $T_{\phi,k}(j) = T_{\phi,k}^+(j) - T_{\phi,k-1}^+(j)$

Similarly, define

$$T_0^+(j) = \inf\{t : (n_t(j), \epsilon_t(j)) = (\bar{N}, +1)\}$$

and then recursively define for $k \geq 1$

$$\begin{aligned} T_k^-(j) &= \inf\{t > T_{k-1}^+(j) : (n_t(j), \epsilon_t(j)) = (N_\phi, -1)\} \\ T_k^+(j) &= \inf\{t > T_k^-(j) : (n_t(j), \epsilon_t(j)) = (\bar{N}, +1)\}. \end{aligned}$$

We note that $T_k^-(j)$ corresponds to the time of the k -th restart from π_0 on machine j and

$$\mathcal{T}_t(j) = \max\{k : T_k^-(j) \leq t\}.$$

We have $\mathcal{T}_t(j)$ is a delayed renewal process counting the number of times a sample travels from chain \bar{N} (targeting π_0) to chain N_1 (targeting π_1) with inter-arrival times $T_k(j) = T_k^-(j) - T_{k-1}^-(j)$.

Although it is possible for a sample to travel from q_ϕ to π_1 and then to π_0 before returning to q_ϕ , note that we are not double-counting or missing any restarts by including two renewal processes. More importantly, by introducing two renewal processes (instead of one), we ensure that the times between successive restarts from a given reference on each machine are independent and identically distributed.

In particular, under Assumption A.2, the inter-arrival times $\{T_{\phi,k}(j)\}_k$, and $\{T_k(j)\}_k$ for $\mathcal{T}_{\phi,t}(j)$ and $\mathcal{T}_t(j)$ respectively are i.i.d. for each machine j with distributions T_ϕ and T respectively. The round trip rate is thus,

$$\begin{aligned}\bar{r}_\phi(\bar{\mathcal{B}}_\phi, \bar{N}) &= \lim_{t \rightarrow \infty} \frac{1}{t} \mathbb{E}[\mathcal{T}_{\phi,t} + \mathcal{T}_t] \\ &= \sum_{j=0}^{\bar{N}} \lim_{t \rightarrow \infty} \frac{1}{t} \mathbb{E}[\mathcal{T}_{\phi,t}(j)] + \sum_{j=0}^{\bar{N}} \lim_{t \rightarrow \infty} \frac{1}{t} \mathbb{E}[\mathcal{T}_t(j)] \\ &= \frac{\bar{N} + 1}{\mathbb{E}[T_\phi]} + \frac{\bar{N} + 1}{\mathbb{E}[T]},\end{aligned}\tag{10}$$

where the last equality follows from the renewal theorem. We find an expression for $\mathbb{E}[T_\phi]$ and argue the form for $\mathbb{E}[T]$ by symmetry. As in [5], we omit the j index for the machine number and define T^{π_1} and T^{q_ϕ} as the first time on a machine where the index reaches $n_t = N_\phi$ and $n_t = 0$ respectively:

$$\begin{aligned}T^{\pi_1} &= \min\{t : (n_t, \epsilon_t) = (N_\phi, 1)\} \\ T^{q_\phi} &= \min\{t : (n_t, \epsilon_t) = (0, -1)\}.\end{aligned}$$

We define $A_{n,\epsilon}^{\pi_1}$ and $A_{n,\epsilon}^{q_\phi}$ to be the expected time for a machine with index process initialized at $(n_0, \epsilon_0) = (n, \epsilon)$, to reach π_1 and q_ϕ respectively,

$$\begin{aligned}A_{n,\epsilon}^{\pi_1} &= \mathbb{E}[T^{\pi_1} | n_0 = n, \epsilon_0 = \epsilon] \\ A_{n,\epsilon}^{q_\phi} &= \mathbb{E}[T^{q_\phi} | n_0 = n, \epsilon_0 = \epsilon].\end{aligned}$$

We can decompose the expected inter-arrival time $\mathbb{E}[T_\phi]$ as at the expected time for a machine to travel from q_ϕ to π_1 plus the expected time to travel from π_1 to q_ϕ ,

$$\mathbb{E}[T_\phi] = A_{0,-1}^{\pi_1} + A_{N_\phi,+1}^{q_\phi}.\tag{11}$$

Also, for notation convenience, we redefine r_n , as the probability of a swap is accepted and respectively rejected between machines with annealing parameter $\bar{\beta}_{n-1}$ and $\bar{\beta}_n$.

Lemma E.1.

$$A_{0,-1}^{\pi_1} = N_\phi + 1 + 2 \cdot \sum_{n=1}^{N_\phi} n \cdot \frac{r_n}{1 - r_n}.\tag{12}$$

Proof of Lemma E.1. Note that by definition, $A_{0,-1}^{\pi_1} = \mathbb{E}[T^{\pi_1} | (n_0, \epsilon_0) = (0, -)]$. Because it is impossible for the index process to reach chains $N_\phi + 1, N_\phi + 2, \dots, \bar{N}$ before time T^π , these chains do not enter the calculations for $A_{0,-1}^{\pi_1}$. Therefore (12) is the same expression for “ $a_\uparrow^{0,-}$ ” as in [5] but with N replaced by N_ϕ . \square

Lemma E.2.

$$A_{N_\phi,+1}^{q_\phi} = 2(\bar{N} + 1) - (N_\phi + 1) + 2 \cdot \sum_{n=1}^{N_\phi} (\bar{N} + 1 - n) \cdot \frac{r_n}{1 - r_n}.$$

Proof of Lemma E.2. It follows from the proof of Theorem 1 in [5] that for $p \in \{\pi_1, q_\phi\}$, and $1 \leq n \leq \bar{N}$, $A_{n,\epsilon}^p$ satisfies the following recursive relation,

$$A_{n,+1}^p - A_{n-1,+1}^p = r_n(A_{n,+1}^p - A_{n-1,-1}^p) - 1\tag{13}$$

$$A_{n,-1}^p - A_{n-1,-1}^p = r_{n-1}(A_{n,+1}^p - A_{n-1,-1}^p) + 1.\tag{14}$$

If we define C_n^p and D_n^p ,

$$C_n^p = A_{n,+1}^p + A_{n-1,-1}^p\tag{15}$$

$$D_n^p = A_{n,+1}^p - A_{n-1,-1}^p.\tag{16}$$

By adding and subtracting (13) and (14), we get the joint recursion in C_n^p and D_n^p , for $n = 1, \dots, \bar{N}$:

$$C_{n+1}^p - C_n^p = r_{n+1}D_{n+1}^p + r_n D_n^p, \quad (17)$$

$$(1 - r_n)D_n^p = (1 - r_{n+1})D_{n+1}^p + 2. \quad (18)$$

If the machine's index process is initialized at $(n_0, \epsilon_0) = (0, -1)$, then $A_{0,-1}^{q\phi} = 0$. We can then substitute in $n = 1$ into (15) and (16) to get,

$$C_1^{q\phi} = D_1^{q\phi}. \quad (19)$$

Similarly if the machine's index process is initialized at $(n_0, \epsilon_0) = (\bar{N}, +1)$, then $A_{\bar{N},+1}^{q\phi} = 1 + A_{\bar{N},-1}^{q\phi}$. We can substitute this into (14) for $n = \bar{N}$ to get,

$$(1 - r_{\bar{N}})D_{\bar{N}}^{q\phi} = 2.$$

Using recursion (18), we find for $n = 1, \dots, \bar{N}$,

$$(1 - r_n)D_n^{q\phi} = 2(\bar{N} + 1 - n).$$

By adding (15) and (16), that for $1 \leq n \leq \bar{N}$,

$$2A_{n,+1}^p = C_n^p + D_n^p. \quad (20)$$

We can decompose $C_n^{q\phi}$ as a telescoping sum, and use (17) within initial condition (19) to get the following expression for $2A_{n,+1}^{q\phi}$ in terms of $D_n^{q\phi}$

$$\begin{aligned} 2A_{N_\phi,+1}^{q\phi} &= C_n^{q\phi} + D_n^{q\phi} \\ &= C_1^{q\phi} + D_n^{q\phi} + \sum_{n=1}^{N_\phi-1} (C_{n+1}^{q\phi} - C_n^{q\phi}) \\ &= D_1^{q\phi} + D_{N_\phi}^{q\phi} + \sum_{n=1}^{N_\phi-1} (r_{n+1}D_{n+1}^{q\phi} + r_{N_\phi}D_{N_\phi}^{q\phi}) \\ &= (1 - r_1)D_1^{q\phi} + (1 - r_{N_\phi})D_{N_\phi}^{q\phi} + 2 \sum_{n=1}^{N_\phi} r_n D_n^{q\phi} \\ &= 2\bar{N} + 2(\bar{N} + 1 - N_\phi) + 2 \sum_{n=1}^{N_\phi} 2(\bar{N} + 1 - n) \frac{r_n}{1 - r_n}. \end{aligned}$$

We arrived at the last line by using (20). Therefore, by dividing by 2 we arrive at our result. \square

By combining Lemma E.1 and Lemma E.2, and using Eq. (11),

$$\begin{aligned} \mathbb{E}[T_\phi] &= A_{0,-1}^{\pi_1} + A_{N_\phi,+1}^{q\phi} \\ &= 2(\bar{N} + 1) + 2(\bar{N} + 1) \sum_{n=1}^{N_\phi} \frac{r_n}{1 - r_n}. \end{aligned} \quad (21)$$

By symmetry, we can repeat the same calculation to compute $\mathbb{E}[T]$, the expected restart time for π_0 to get,

$$\mathbb{E}[T] = 2(\bar{N} + 1) + 2(\bar{N} + 1) \sum_{n=N_\phi+1}^{\bar{N}} \frac{r_n}{1 - r_n}. \quad (22)$$

Therefore, Eq. (21) and Eq. (22) in Eq. (10) imply that

$$\begin{aligned} \bar{\tau}_\phi(\bar{\mathcal{B}}_{\phi,\bar{N}}) &= \frac{\bar{N} + 1}{\mathbb{E}[T_\phi]} + \frac{\bar{N} + 1}{\mathbb{E}[T]} \\ &= \frac{1}{2 + 2 \sum_{n=1}^{N_\phi} \frac{r_n}{1 - r_n}} + \frac{1}{2 + 2 \sum_{n=N_\phi+1}^{\bar{N}} \frac{r_n}{1 - r_n}} \\ &= \tau_\phi(\mathcal{B}_{\phi,N_\phi}) + \tau(\mathcal{B}_N). \end{aligned}$$

Finally, it follows from Theorem 3 in [5], that as $\|\mathcal{B}_N\|, \|\mathcal{B}_{\phi, N_\Phi}\| \rightarrow 0$ we have

$$\begin{aligned}\lim_{N_\phi \rightarrow \infty} \tau_\phi(\mathcal{B}_{\phi, N_\phi}) &= \frac{1}{2 + 2\Lambda(q_\phi, \pi_1)} \\ \lim_{N \rightarrow \infty} \tau(\mathcal{B}_N) &= \frac{1}{2 + 2\Lambda(\pi_0, \pi_1)}.\end{aligned}$$

Therefore, as $\|\bar{\mathcal{B}}_{\phi, \bar{N}}\| \rightarrow 0$ chain-asymptotic restart rate satisfies,

$$\lim_{\bar{N} \rightarrow \infty} \bar{\tau}_\phi(\bar{\mathcal{B}}_{\phi, \bar{N}}) = \frac{1}{2 + 2\Lambda(q_\phi, \pi_1)} + \frac{1}{2 + 2\Lambda(\pi_0, \pi_1)}.$$

	Inference problem	n	d	$\hat{\Lambda}(\pi_0, \pi_1)$
Synthetic	Product	100,000	2	3.7
	Simple-Mix (collapsed)	300	5	4.3
	Elliptic	100,000	2	4.4
	Toy-Mix	NA	1	9.3
Real data	Transfection	52	5	6.4
	Titanic	887	9	7.7
	Rockets (collapsed)	5,667	2	3.4
	Challenger	23	2	4.2
	Change-point	109	7	3.3
	Vaccines	77,828	12	7.8
	Lip Cancer	536	60	15
	Pollution	22,548	275	56.9
	8 schools	8	10	0.8
	Phylogenetic inference	249	10,395	7.0
	Spring failure (improper prior)	10	1	Not defined

Table 1: Summary of the models considered in this paper. The sample size n , number of model parameters d , and fixed reference GCB $\hat{\Lambda}(\pi_0, \pi_1)$ (defined for models with a proper prior distribution). The label ‘‘collapsed’’ is used for the models that are based on [5] but with some latent variables analytically marginalized.

F Details of experiments

F.1 ODE parameters (mRNA transfection data)

The first data set that we consider (‘‘Transfection’’) is a time series data set based on mRNA transfection data and an ordinary differential equation (ODE) model [4]. The data are observations O_t at times $t = 1, 2, \dots, 52$ modelled as $O_t | k_{m_0}, \delta, \beta, t_0, \sigma \sim N(\mu, \sigma^2)$ where $k_{m_0}, \delta, \beta, t_0, \sigma$ are parameters and

$$\mu = \frac{k_{m_0}}{\delta - \beta} (1 - \exp(-(\delta - \beta) \cdot (t - t_0)) \cdot \exp(-\beta \cdot (t - t_0))).$$

The priors placed on the parameters are all log-uniform (i.e., distributed according to 10^U where U denotes a random variable with a uniform distribution on $[a, b]$). Specifically, $k_{m_0}, \delta, \beta \sim \text{LogUniform}(-5, 5)$, $t_0 \sim \text{LogUniform}(-2, 1)$, and $\sigma \sim \text{LogUniform}(-2, 2)$, with all parameters a priori independent. We use 50 PT chains, unless stated otherwise. Data is included in the supplement under `bl-vpt/data/m_rna_transfection/processed.csv`.

F.2 GLM (Titanic data)

Next, we consider a binary generalized linear model (‘‘Titanic’’) with binary response data, Y_i , indicators of survival for the i -th Titanic passenger, along with several covariates, \mathbf{x}_i . We assume that $Y_i | \beta_0, \beta_1, \mathbf{x}_i \sim \text{Bernoulli}(1/(1 + \exp(-(\beta_0 + \beta_1^\top \mathbf{x}_i))))$. Note that this example is similar to the one used by [5] although our prior differs in that we assume that $\beta_0, \beta_{1,1}, \beta_{1,2}, \dots, \beta_{1,7} \sim \text{Cauchy}(\sigma)$ with scale parameter σ . Further, $\sigma \sim \text{Exp}(1)$. All parameters are assumed to be independent in the prior. We use 30 PT chains, unless stated otherwise. Data is included in the supplement under `bl-vpt/data/titanic`.

F.3 Unidentifiable product

The unidentifiable product model (‘‘Product’’) is an artificial data set of size $n = 100,000$. The number of failures of an experiment, n_f , given the number of trials n_t and parameters x and y is modelled as $n_f | n_t, x, y \sim \text{Bin}(n_t, x \cdot y)$. We place priors $X, Y \sim U(0, 1)$ and set $n_t = 100,000$. We observe $n_f = 50,000$ failures. For this model, $d = 2$. Due to identifiability, the posterior concentrates on a thin curve in the square $[0, 1] \times [0, 1]$. We use 15 PT chains, unless stated otherwise.

F.4 Mixture model

We consider a multi-modal posterior that arises from a normal mixture model (“Simple-Mix”). We model data $X_1, X_2, \dots, X_m | \mu_1, \mu_2, \sigma_1, \sigma_2, \pi \sim \pi \cdot N(\mu_1, \sigma_1^2) + (1 - \pi) \cdot N(\mu_2, \sigma_2^2)$ with priors $\mu_1, \mu_2 \sim N(150, 100^2)$, $\sigma_1, \sigma_2 \sim U(0, 100)$, and $\pi \sim U(0, 1)$. Due to the label-switching problem, the resulting posterior is multi-modal. In all the experiments we marginalize over the mixture model indicator variables in contrast to [5]. We use 10 PT chains, unless stated otherwise. Data is included in the supplement under `VariationalPT/data/simple-mix.csv`.

F.5 Bayesian hierarchical model

We also consider a Bayesian hierarchical model based on rocket launch failure data (“Rockets”). The number of rocket launch failures, f_r , along with the total number of rocket launches, l_r , for $R = 367$ types of rockets is obtained. Given the probability of rocket launch failure for rocket r , we model $f_r | \pi_r, l_r \sim \text{Bin}(l_r, \pi_r)$. Given parameters m and s , we model $\pi_r | m, s \sim \text{Beta}(m, s, (1 - m)s)$ and use the hyper-prior $m \sim U(0, 1)$ and $s \sim \text{Exp}(0.1)$ (rate parameter). In this example we perform inference over each of the π_r and m, s so that $d = 369$ and $n = 5,667$. In all the experiments we marginalize over the random effects in contrast to [5]. We use 10 PT chains, unless stated otherwise. Data is included in the supplement under `bl-vpt/data/failure_counts.csv`.

F.6 Weakly identifiable elliptic curve

A weakly identifiable model is also considered (“Elliptic”). This data set is an artificial data set with the number of failures of an experiment, n_f , given the number of trials n_t and parameters x, y modelled as $n_f | n_t, x, y \sim \text{Bin}(n_t, p(x, y))$ where

$$p'(x, y) = y^2 - x^3 + 2x - 0.5$$
$$p(x, y) = \begin{cases} 0 & p'(x, y) < 0 \\ 1 & p'(x, y) > 1 \\ p'(x, y) & \text{otherwise.} \end{cases}$$

We observe $n_t = 100,000$ trials and $n_f = 50,000$ failures. We use the prior $X, Y \sim U(-3, 3)$. We use 30 PT chains, unless stated otherwise.

F.7 GLM (Challenger data)

Another GLM but applied to Challenger shuttle O-ring data (“Challenger”). The responses consist of binary indicator variables for incidents, Y_i , for 23 shuttle launches at temperatures x_i . We model the responses as $Y_i | x_i, \beta_0, \beta_1 \sim \text{Bern}(1/(1 + \exp(-(\beta_0 + \beta_1 x_i))))$ and use the prior $\beta_0, \beta_1 \sim N(0, 100)$. We use 15 PT chains, unless stated otherwise. Data is included in the supplement under `bl-vpt/data/challenger`.

F.8 Additional Blang models

We have implemented the models in Sections F.1–F.7 both procedurally in Julia and declaratively in the Blang probabilistic programming language (PPL) [26] to ensure agreement of the results. We then implemented additional models in Blang, briefly described in this section, to illustrate that the proposed method can be seamlessly incorporated into a PPL. To see more details on these additional models (as well as those described in Sections F.1–F.7), see their PPL source code in the sub-directory `bl-vpt/src/main/java/ptbm/models/` of the supplement.

Lip Cancer and Pollution: a sparse Conditional Auto Regressive (CAR) Poisson regression spatial model, constructed as in <https://mc-stan.org/users/documentation/case-studies/mbjoseph-CARStan.html> (full model available in `bl-vpt/src/main/java/ptbm/models/SparseCAR.bl`). For the Lip Cancer problem, we use the dataset documented in the R package `CARBAYesdata`, see `bl-vpt/data/scotland_lip_cancer` in the supplement for more information on preprocessing. The Pollution problem is based on the same model but with the bigger dataset documented in `bl-vpt/data/pollution_health`, also obtained from the `CARBAYesdata` package on CRAN, which is under a GPL-2 / GPL-3 license. This

provides some examples of how the global communication barrier can be decreased in a realistic data analysis scenario: in the first dataset, from 15 to 6, and in the second, from 57 to 7. For the Pollution dataset, we found the GCB to decrease substantially after considering a larger number of tuning rounds with 4 million PT scans. The GCB with the variational reference during each of the tuning rounds for this model is presented in Fig. 6.

Vaccines: the data (`bl-vpt/data/vaccines/data.csv`) consists in the following Phase III COVID-19 vaccines clinical trials: Pfizer-BioNTech, Moderna-NIH, and two AZ-Oxford trials ('South Africa B.1.351' and 'Combined'). The number of cases in each arm of each trial is modelled using a binomial. In each control arm, the probability parameter is set to a trial-specific incidence parameter. In each 'treatment' arm, the probability parameter is set to the same incidence parameter multiplied by one minus a trial-specific efficacy parameter. While the incidence and efficacy parameters are trial specific, the parameters of these distributions are tied across the four trials (full model available in `bl-vpt/src/main/java/ptbm/models/Vaccines.bl`).

Change-point: a time series model of discrete counts. We assume one change point uniformly distributed on the time series. The observations at each time point is negative binomial distributed with one set of parameters for the observations before the change point and one set for after the change point (full model available in `bl-vpt/src/main/java/ptbm/models/Mining.bl`). This model is applied to the dataset of annual numbers of accidents due to disasters in British coal mines for years from 1850 to 1962, considered in Carlin et al. (1992) (`bl-vpt/data/mining-disasters.csv`).

8 schools: the classical problem from Rubin (1981), see `bl-vpt/src/main/java/ptbm/models/EightSchools.bl` and `bl-vpt/data/eight-schools.csv`.

Phylogenetics: The same setup as the *phylogenetic species tree problem* from [5] (`bl-vpt/src/main/java/ptbm/models/PhylogeneticTree.bl`). The data consists in aligned mtDNA sequences (`bl-vpt/data/FES_8.g.fasta`). We only fit variational distributions to the real-valued evolutionary parameters—there is work on constructing variational families for phylogenetic trees [34, 35], but we leave the combination of these families with our inference method for future work.

Spring failure: The density estimation problem for spring failure data described in Davison (2003), example 4.2, with a Cauchy likelihood (`bl-vpt/src/main/java/ptbm/models/ImproperCauchy.bl`). We use the Lebesgue improper prior for the Cauchy likelihood's location parameter. This illustrates another use case for our method: when standard PT is applied to a model with an improper prior, one has to select $\beta_0 > 0$ such that $\beta > \beta_0$ guarantees that π_β is a (normalizable) probability distribution, moreover it is in general not possible to get i.i.d. samples from π_{β_0} . In contrast, our method works with $\beta_0 = 0$ and allows i.i.d. sampling from the variational chain. In the stabilized variant, for the non-adaptive "leg" one can use a fixed variational parameter instead of π_0 . Results for this model are shown in Fig. 7.

ToyMix: the density $f(x) = 0.5\phi(x; -r, 0.01) + 0.5\phi(x; r, 0.01)$ where $\phi(\cdot; \mu, \sigma^2)$ is the normal density (`bl-vpt/src/main/java/ptbm/models/ToyMix.bl`). We use $r = 10$.

F.9 Markovian score climbing

For the Transfection model, we implemented the Markovian score climbing (MSC) algorithm of [27]. In the MSC algorithm, there are three main tuning parameters: the number of tuning rounds K , the number of samples used in each tuning round S , and the step size (or step size sequence) ϵ . The inputs to the algorithm also include the starting values of the variational parameters λ_0 , and the starting sample observation z_0 . For the mean-field normal variational references, we use the marginal means and log standard deviations as the variational parameters so that all parameters can take on values in \mathbb{R} . We initialize each of the log standard deviation parameters to $\log(100.0)$. For the mean parameters, we initialize them to $(1.0, 1.0, 1.0, 0.32, 1.0)$, which are also the initial values provided to the MCMC samplers in the PT algorithms. We use $K = 100,000$ tuning rounds with $S = 100$ and a step size of $\epsilon = 0.0005$. The initial sample provided is the vector of initial mean parameters. The MSC experiments are run 10 times for each selection of simulation settings.

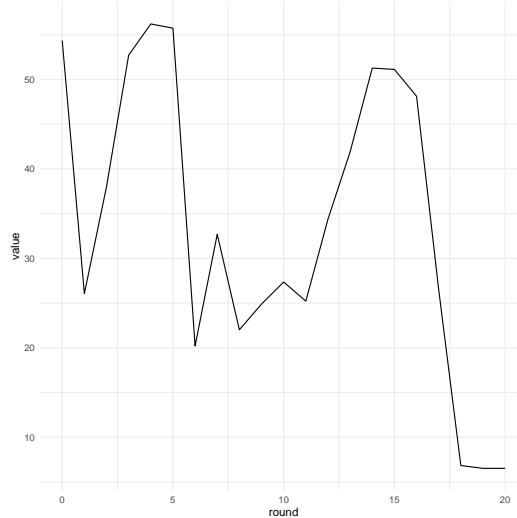


Figure 6: Global communication barrier for the Pollution model in the variational reference chain during each of the tuning rounds. The GCB for the fixed reference chain is estimated to be 57.

Initially, we tried larger values of the step size parameters, starting at $\epsilon = 0.1$. However, we observed that the estimated variational parameters jumped around a large range of values. We therefore decreased the value of ϵ until there were no convergence issues (i.e., no exceptionally large gradients and the variational parameter estimates seemed to converge based on plots of the parameter estimates against the tuning round number). We also ran the experiment with a smaller step size of $\epsilon = 0.00025$. However, we noticed that the variational parameter estimates displayed a similar behaviour: the parameter estimate would center on only one of the two modes.

F.10 Additional Details

We use the same number of chains in each leg of variational PT with two reference distributions. For ESS calculations in Julia, we use all samples from the target distribution, including those obtained during annealing schedule and variational reference tuning rounds. For the implementation of variational PT with two references, we employ two separate PT chains: one with a fixed reference and one with a variational reference. During each tuning round, samples from the target distribution in each chain are pooled together to estimate the variational parameters for the reference distribution. In Blang, we implement the topology in which the target distributions between the instances of PT are connected. More information about these different topologies can be found in Appendix F.11.3. In the Julia implementation of the variational PT algorithm, the covariance matrices for the Gaussian reference are estimated using the functions `std()` and `cov()`. The estimates of the variance therefore differ by a factor of $n/(n-1)$ compared to the MLE estimates where n is the sample size for parameter estimation.

All experiments use the same exploration kernel, namely a slice sampling algorithm with “doubling and shrinking” [36, Sections 4.1–4.2]. We performed preliminary experiments with HMC. However, we found that having to tune one HMC sampler for each annealed chain was onerous. We leave the problem of adapting several annealed exploration kernels to future work. Slice sampling in contrast does not have sensitive tuning parameters that require tuning. For the initial state in each chain for the simulations of Section 4.1, the same state is used for all PT initializations for the different seeds. The initial state was chosen to lie in a region with positive density with respect to the reference and target distributions.

Unless mentioned otherwise, all PT algorithms use Deterministic Even Odd (DEO) swaps and the NRPT adaptive schedule algorithm. See [5] for details. Julia simulations were run on an Intel i9-10900K processor with 32 GB of RAM. We also acknowledge use of the ARC Sockeye computing platform (Gold and Silver Xeon 2.1 GHz processors) from the University of British Columbia.

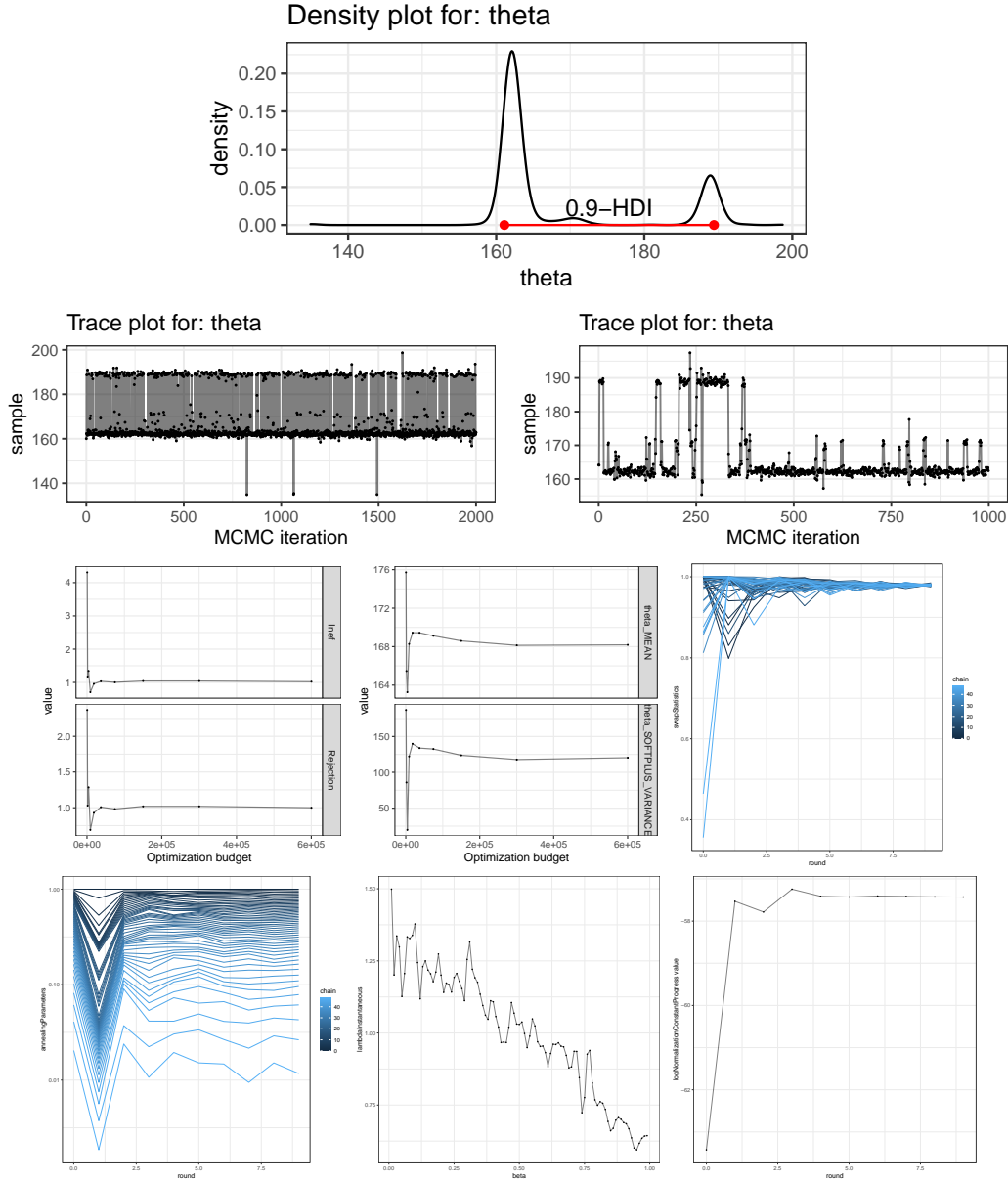


Figure 7: Stabilized variational PT applied to a density estimation problem with a Cauchy likelihood and an improper prior (Section F.8). **First row:** post-burn-in approximation of the posterior distribution over the location parameter θ . Multi-modality is clearly visible. **Second row, left:** trace plot of the same parameter obtained from stabilized variational PT. The stabilized variational PT algorithm is able to frequently switch modes. **Second row, right:** same trace plot but obtained from a single chain MCMC algorithm with the same exploration kernel. **Third row, left:** estimates of two objective functions as a function of the adaptation rounds (“Inef” refers to the sum of the rejection odds, “Rejection,” to the sum of rejection rates). **Third row, center:** value of the variational parameters as a function of the adaptation round. The facet “theta_MEAN” refers to the mean of the variational normal distribution approximating the posterior on θ , and “theta_SOFTPLUS_VARIANCE”, to the (reparameterized) variance parameter of the same variational distribution. **Third row, right:** average swap acceptance probabilities for the $N = 50$ chains as a function of the adaptation round. **Bottom row, left:** each chain’s β_i as a function of the adaptation round. **Bottom row, center:** estimated local communication barrier. Even with the relatively large number of chains used in this example, it appears intrinsically less smooth than for the other examples considered in this paper. This may be due to the heavier likelihood tails used in this example. **Bottom row, right:** estimated normalization constant based on the stepping stone method as a function of the adaptation round.

F.11 Additional experimental results

F.11.1 Additional plots

Additional plots accompanying the results of Section 4.1 are presented in Fig. 8 and Fig. 9. Additional plots for the Cauchy example can be found in Fig. 7. For these figures, the local communication barrier (LCB) between π_0 and π_1 at $\beta \in [0, 1]$ is

$$\lambda(\pi_0, \pi_1, \beta) = \frac{1}{2} \mathbb{E}[|\ell(X_\beta) - \ell(X'_\beta)|], \quad \ell(x) = \log \frac{\pi_1(x)}{\pi_0(x)}, \quad X_\beta, X'_\beta \stackrel{\text{i.i.d.}}{\sim} \pi_\beta.$$

The LCB can be viewed as an instantaneous communication barrier for each point along the path between π_0 and π_1 . The integral of the LCB yields the GCB under appropriate moment conditions.

F.11.2 Additional results comparing stochastic gradient optimization and moment matching

This section provides additional details for the results described in Section 4.2.

For the stochastic gradient experiments, we considered optimizing several surrogate functions in addition to the global communication barrier (GCB). The first one is the SKL objective, which was used in [37] as a GCB surrogate for optimizing the path between a fixed reference and the target. An estimator of the gradient of the SKL is derived in [37]. We also considered a straightforward variant of this estimator for the forward KL objective. Even when considering a surrogate objective function, we measure performance using the quantity we are ultimately interested in, the GCB, estimated using the sum of the communication rejection rates. Methods optimizing the GCB are labelled ‘Rejection’ to emphasize that they are technically optimizing the sum of rejections.

We compared the following optimization algorithms: the moment matching method described in Section 3, basic stochastic gradient descent (SGD), where we update variational parameters using the formula $\phi^{(i+1)} \leftarrow \phi^{(i)} - \alpha(i+1)^{-0.6} g^{(i)}$, following [38, Section 4], where $g^{(i)}$ is the stochastic gradient estimate, and Adam [39]. We found both SGD and Adam to be sensitive to the scale α of the updates (where α is defined above for SGD, and a similar parameter appears in Adam, also denoted α in [39]), which we varied in the grid $1/100, 1/10, 1, 10$ (this grid was iteratively increased starting at 1 until the optima laid inside the grid).

We re-parameterized the variance parameters to lie in the real line using a differentiable transformation, which we set to the soft-plus transformation, $\log 1p(\exp(x))$. All methods use the same exploration kernel (Section F.10), which is the expensive inner loop of all optimization methods considered, so we use the number of exploration kernel applications as a model for computational time (abscissa for all plots in this subsection). To set the number of chains, we used the heuristic in [5, Section 5.3], $N^* \approx 2\Lambda$. We estimated $\Lambda \approx 3.5$ and used 8 chains for these experiments. For the stochastic optimization methods, we based the estimator of the gradient on 20 samples each interspersed with one scan, where a scan consists in one application of the local exploration kernel to each variable in each chains, and one set of odd or even swaps.

Simultaneous optimization of the annealing schedule and the variational parameters is straightforward with our moment matching scheme: this is done using Algorithms 2 and 3 in [5] which, like our scheme, proceed in rounds and hence can be performed in combination with round-based variational moment matching. Therefore, for all experiments involving moment matching, we learn an optimal schedule from scratch (i.e., initialized at an equally spaced schedule). For the stochastic optimization methods, simultaneous optimization of annealing schedules is more involved. The GCB is not a suitable objective, as when the number of chains gets larger, the GCB is asymptotically invariant to the schedule (provided the mesh size goes to zero, see [5, Corollary 2]). It would be possible to use the scheme of [38], however this would add more tuning parameters. Instead, for these experiments, we provide all stochastic optimization methods with an optimally tuned schedule and exclude the cost of creating this optimal schedule from the computational budget calculation. As we shall see even with this head start, stochastic optimization does not perform as well as moment matching.

Our implementations of SGD and Adam are augmented with a form of error recovery: when a parameter update leads to a variational parameter where the GCB estimate is not finite (e.g. due to underflow or overflow), we roll back to the previous parameter value. Our implementation stores only one previous valid parameter setting to avoid keeping a history in memory. As a result, some of the stochastic optimization methods move to regions where with high probabilities the proposed next

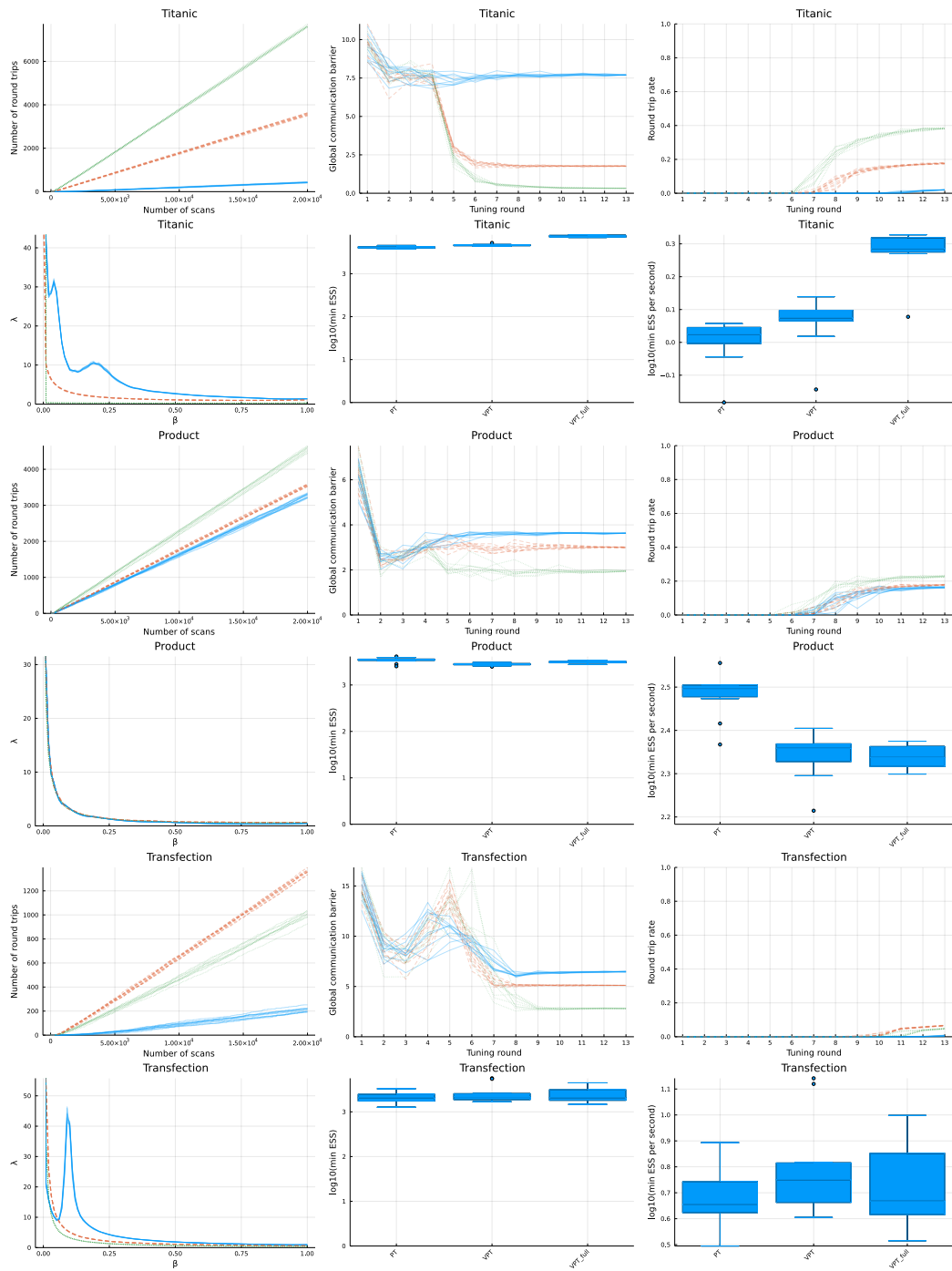


Figure 8: Number of round trips, GCB, round trip rate, local communication barrier (LCB), ESS, and ESS per second. Green/red: Full-covariance/mean-field variational PT. Blue: NRPT.

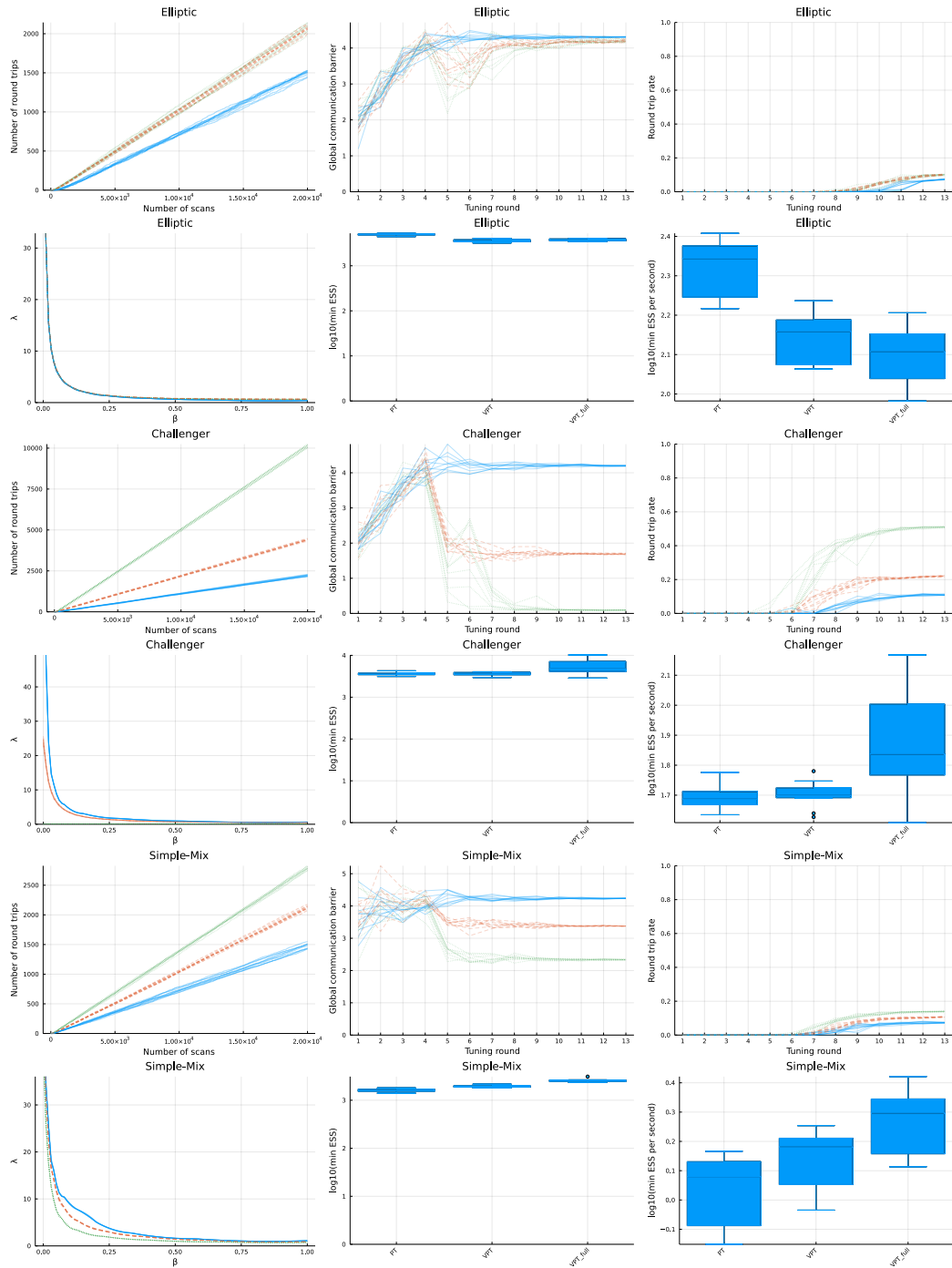


Figure 9: Number of round trips, GCB, round trip rate, LCB, ESS, and ESS per second. Green/red: Full-covariance/mean-field variational PT. Blue: NRPT.

position leads to a rollback—this occurs especially when the step size scale is too large, as shown in Fig. 11. More precisely, this occurs with Adam+FKL for scales larger than 1, with Adam+GCB for all scales considered, with SGD+GCB for scales larger than 0.1, and for all SKL methods for scales larger than 1. We show in Fig. 12 the mean GCB objective, averaged over the finite values (individual traces shown in Fig. 13).

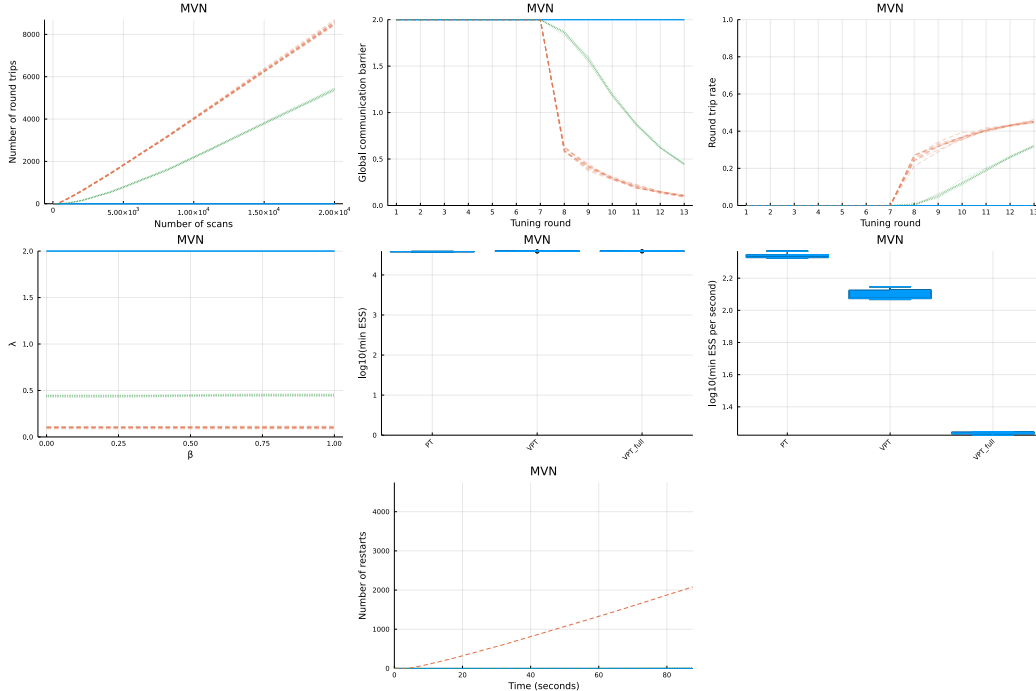


Figure 10: Results for the 100-dimensional multivariate normal target distribution.

Among the configurations that did not lead to non-finite values, the following methods eventually achieved the same optimal GCB loss within the total optimization budget: Adam+FKL+0.01, Adam+FKL+0.1, SGD+SKL+1, Adam+SKL+0.01, Adam+SKL+0.1, SGD+SKL+1. Among those, the fastest to reach that value were Adam+SKL+0.1 and Adam+FKL+0.1, with roughly equivalent performances.

We applied these best performing settings, Adam+SKL+0.1 and Adam+FKL+0.1, to two other problems to see how well they generalize. The two additional problems are: a Bayesian GLM model applied to the titanic dataset described in Section F.2 (with the only difference that we use normal priors here instead of Cauchy priors), and the change point problem described in Section F.8. We use the same experimental conditions as those described above for the Bayesian hierarchical model, with the difference that for the logistic regression problem we used a larger number of chains (20) to take into account the larger GCB (≈ 8). The results are shown in Section 4.2 and demonstrate that stochastic optimization tuning does not generalize well from one problem to another, while moment matching performs well without requiring tuning.

To replicate the results in this subsection, run, from the root of the repository `bl-vpt-nextflow` at <https://github.com/UBC-Stat-ML/bl-vpt-nextflow> the command `./nextflow run optimization.nf` and the results will be produced in the directory `bl-vpt-nextflow/deliverables/optimization`.

F.11.3 Additional results comparing different PT topologies across several models

In this section, we perform an exhaustive empirical comparison of different PT algorithms incorporating a variational distribution. We also include a baseline consisting of PT with a fixed reference. Based on the results of the previous section, we perform optimization using moment matching.

In all experiments in this subsection, we use a normal variational family with diagonal covariance. This ensures that the running time is dominated by the local exploration kernels. We also ensure that the total number of chains is the same for all methods considered. It follows that one scan has comparable running time for all methods considered in this subsection.

To describe the PT algorithms we use the following notation: we use \mathbf{T} to denote the target distribution; \mathbf{F} , to denote a fixed reference distribution; \mathbf{V} , to denote a variational distribution. We use a star

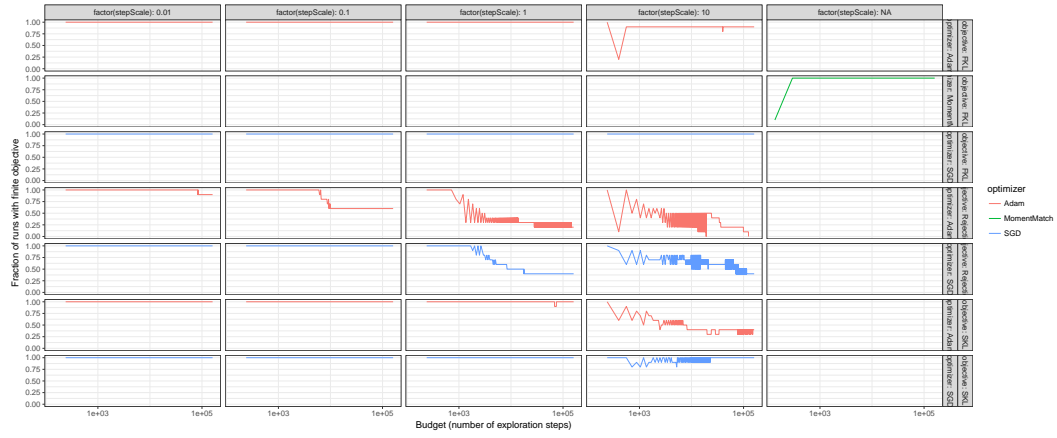


Figure 11: Fraction of the 10 replicates (each provided with a different random seed) that have a finite objective function at each optimization iteration.

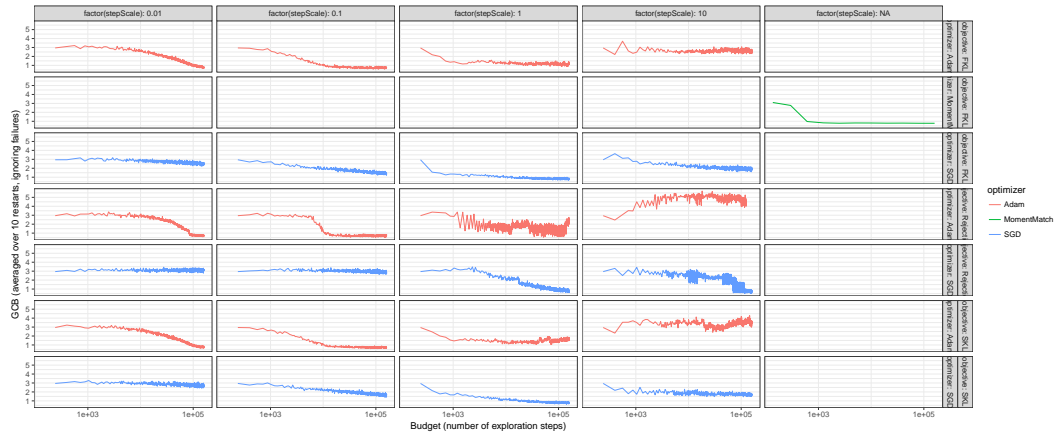


Figure 12: Aggregated performance of all optimization methods and surrogate functions considered in this work.

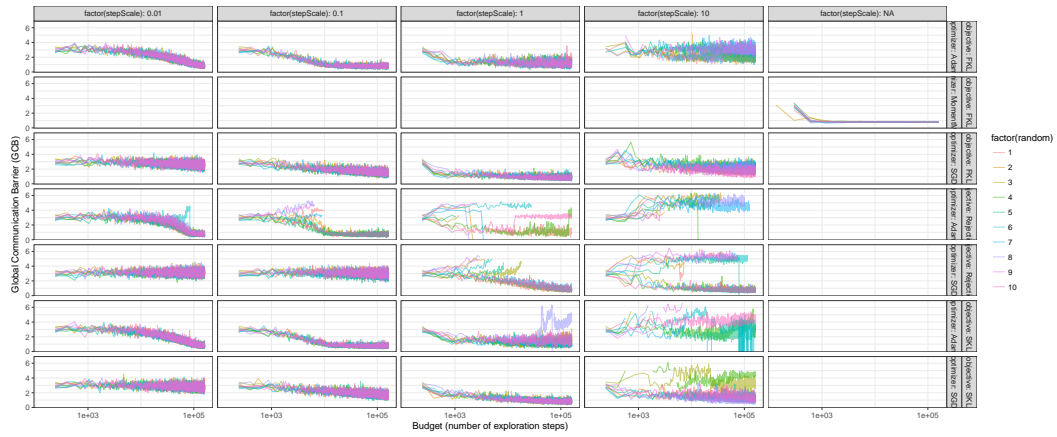


Figure 13: Performance traces of individual optimizers provided with different random seeds (colours).

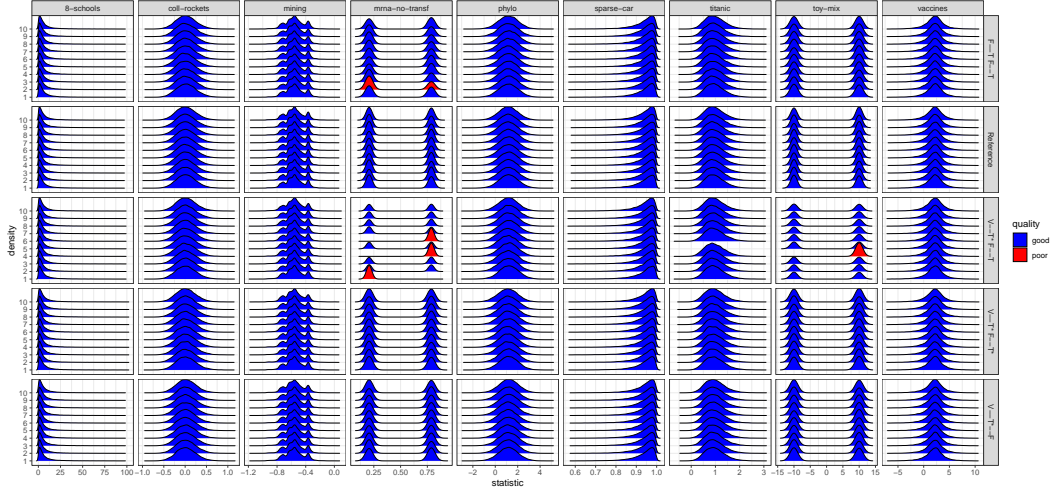


Figure 14: For each model (column), we selected a key statistic or parameter. We show here the approximations of the marginal posterior distributions of these key statistics, for the different algorithms (rows) and 10 random seeds. Those in red have Kolmogorov-Smirnov (KS) distance greater than 0.1 compared to the “Reference.”

superscript to indicate which chain(s) are used to collect samples for moment matching when updating the variational distribution. Using this notation, the algorithms considered are:

“**F—T F—T**”: two independent, non-interacting copies of standard PT. We use two copies in order to have a comparable running time per MCMC scan.

“**V—T* F—T**”: a basic variational approximation (**V—T***), with one independent, non-interacting standard PT, added to have comparable running time per MCMC scan.

“**V—T* F—T***”: a first type of stabilized variational approximation PT algorithm. As in the algorithm above, it consists of two independent PT algorithms, one using a variational approximation and the other with a fixed reference. In contrast to the one above, the samples from the two PT algorithms are pooled at each round when performing moment-matching.

“**V—T*—F**”: the same algorithm as above, but where the states of the two target distributions are swapped at every second scan in order to maintain non-reversibility of the index process [5, Section 3.4].

“**Reference**”: the same algorithm as “**F—T F—T**”, but with ten times the number of MCMC scans as the other methods.

In the main paper, for simplicity, “**F—T F—T**” is described as “standard PT”; “**V—T* F—T**”, as “basic variational PT”; and “**V—T*—F**”, as “stabilized variational PT.” As shown in this section “**V—T*—F**” and “**V—T* F—T***” have similar performance in terms of restart rate, however the former is more natural and easier to analyze (Theorem 3.6).

We consider the following models in this section, with the number of chains indicated in parentheses (number of chains selected to be approximately 2λ as recommended in [5, Section 5.3]): the eight schools model ($N = 10$), a change point detection model applied on a dataset of mining incidents ($N = 10$), Bayesian estimation of ODE parameters for an mRNA transfection dataset ($N = 30$), Bayesian logistic regression applied to the titanic dataset ($N = 10$), two distinct Bayesian hierarchical models, one for prediction of rocket reliability ($N = 10$) and another tailored to estimating efficacy of multiple COVID-19 vaccines ($N = 20$), one sparse Conditional Auto-Regressive (CAR) spatial model applied to a lip cancer dataset ($N = 20$), one synthetic multi-modal example ($N = 20$), and one phylogenetic inference problem ($N = 20$). Refer to Sections F.1–F.8 for more information.

For each model we first identified one key statistic: either the one of scientific interest or one such that its marginal posterior distribution is multi-modal. We ran each combination of algorithm and model 10 times with different random seeds. The approximations of the marginal posterior distributions are shown in Fig. 14. Visual inspection shows that there are runs that clearly miss the multi-modal

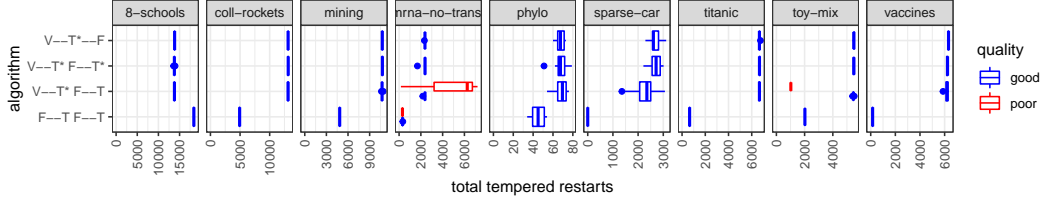


Figure 15: Tempered restarts for different PT algorithms (rows) and models (facets). Each algorithm is executed 10 times with different random seeds. The results are also segregated based on the KS criterion described in Fig. 14.

structure of the problem. To quantify this, we computed the Kolmogorov-Smirnov (KS) distance between the marginal posterior of this statistic obtained from the “**Reference**” run and that obtained from each algorithm. We mark in red the result from any random seed leading to a KS distance greater than 1/10.

Next, we looked at tempered restart count statistics for all combinations of models and algorithms, also splitting the results based on the above mentioned KS threshold. It is important to make this KS-based split, as runs that missed one of the mode may under-estimate the difficulty of the problem and hence over-estimate the number of tempered restarts. The results are shown in Fig. 15 and Table 2.

model	algorithm	# KS<0.1	Q1	Q2	Q3
8-schools	F-T F-T	10	18310	18382	18414
8-schools	V-T* F-T	10	13728	13788	13809
8-schools	V-T* F-T*	10	13718	13770	13797
8-schools	V-T*-F	10	13797	13829	13852
coll-rockets	F-T F-T	10	4876	4931	4953
coll-rockets	V-T* F-T	10	13048	13105	13160
coll-rockets	V-T* F-T*	10	13074	13128	13161
coll-rockets	V-T*-F	10	13081	13108	13151
mining	F-T F-T	10	4824	4848	4863
mining	V-T* F-T	10	10704	10728	10745
mining	V-T* F-T*	10	10700	10766	10823
mining	V-T*-F	10	10716	10750	10798
mrna-no-transf	F-T F-T	9	311	316	320
mrna-no-transf	V-T* F-T	7	2366	2381	2384
mrna-no-transf	V-T* F-T*	10	2361	2378	2414
mrna-no-transf	V-T*-F	10	2366	2376	2385
phylo	F-T F-T	10	40	45	51
phylo	V-T* F-T	10	65	70	73
phylo	V-T* F-T*	10	65	68	72
phylo	V-T*-F	10	65	68	71
sparse-car	F-T F-T	10	0	0	0
sparse-car	V-T* F-T	10	2063	2348	2501
sparse-car	V-T* F-T*	10	2556	2714	2878
sparse-car	V-T*-F	10	2579	2607	2810
titanic	F-T F-T	10	642	650	661
titanic	V-T* F-T	9	6615	6662	6691
titanic	V-T* F-T*	10	6649	6666	6715
titanic	V-T*-F	10	6644	6661	6687
toy-mix	F-T F-T	10	2010	2020	2038
toy-mix	V-T* F-T	9	5443	5458	5469
toy-mix	V-T* F-T*	10	5446	5491	5519
toy-mix	V-T*-F	10	5474	5484	5529
vaccines	F-T F-T	10	147	154	166
vaccines	V-T* F-T	10	6118	6208	6264
vaccines	V-T* F-T*	10	6168	6236	6262
vaccines	V-T*-F	10	6288	6316	6336

Table 2: Quantiles (0.25, 0.5, 0.75) of the number of restarts for the subset of the runs with KS < 0.1.

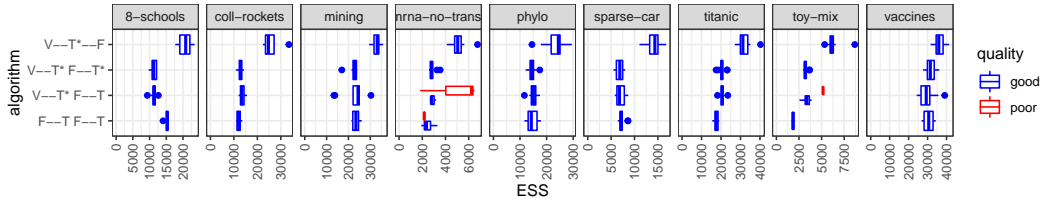


Figure 16: Effective Sample Size (ESS) for each model’s key statistic, for different PT algorithms (rows) and models (facets). Each algorithm is executed 10 times with different random seeds. The results are also segregated based on the KS criterion described in Fig. 14.

In most of the models considered, we observed a large increase in the number of tempered restarts when going from standard PT to variational PT. We observed an increase of a factor ~ 2.5 in the rocket model, ~ 2.2 for the mining problem, ~ 1.6 for the phylogenetic problem, ~ 10.2 for the titanic problem, ~ 40.3 for the vaccine problem (above speed-up estimates computed on the median column of Table 2). The gains are particularly impressive for the sparse CAR model applied to the lip cancer dataset, in which standard PT achieves 0 restarts while the median number of restarts for the variational methods are all higher than 2300 restarts.

For the mRNA and toy mixture problems, only the stabilized algorithms (“ $\mathbf{V-T^*F}$ ” and “ $\mathbf{V-T^* F-T^*}$ ”) succeeded in avoiding catastrophic failures, and compared to standard PT led to an increase in median restarts of a factor ~ 7.5 for the mRNA problem and of a factor ~ 2.7 for the toy mixture problem. In the mRNA example, 3 out of 10 applications of the basic variational method, “ $\mathbf{V-T^* F-T}$ ”, led to a catastrophic failure, and 1 out of 10 in the toy mixture example. Note that the number of restarts is overestimated in the failed runs, highlighting the importance of using a stabilized algorithm.

The 8 schools problem provides an example where a variational approach based on a diagonal covariance matrix underperforms standard PT. In this example, the number of round trips decreased from a median of 18382 to a median of 13788, 13770, and 13829 for the three variational algorithms considered. But note that the drop in performance is less than 50%, which agrees with the result in Theorem 3.6.

Fig. 16 and Table 3 show performance in terms of the effective sample size (ESS) of each model’s key statistic. The ESS is computed using the `mcmcse` R package which implements a batch mean estimator. For the non-interacting variational variants, “ $\mathbf{V-T^* F-T}$ ” and “ $\mathbf{V-T^* F-T^*}$ ”, we observe modest ESS gains compared to standard PT in the rocket, sparse CAR, mRNA and titanic problems, while the gains are larger for the toy mixture problem (~ 1.8 increase). For the interacting variational variant, “ $\mathbf{V-T^*F}$ ”, the gains are substantial in all problems considered. However, in contrast to the other algorithms where adding the ESS of the two copies is justified by independence, the ESS estimator may not be reliable in the case of “ $\mathbf{V-T^*F}$ ” given the interactions. The restart rate does not have this limitation so we recommend gauging the performance of the methods primarily based on their restart rate.

We also show the local and global communication barriers, λ and Λ , for these models and algorithms in Fig. 17 and Fig. 18. Interestingly, in some of the cases, e.g. the transfection problem, the high gains in terms of tempered restarts obtained by going from standard PT to variational, are not as large when measured by Λ . This could be due to the variational λ function being generally smoother and hence the optimal schedule easier to approximate in a finite number of rounds.

To replicate the results in this subsection, run, from the root of the repository `bl-vpt-nextflow` at <https://github.com/UBC-Stat-ML/bl-vpt-nextflow> the command `./nextflow run pt_topologies.nf` and the results will be produced in the directory `bl-vpt-nextflow/deliverables/pt_topologies`.

model	algorithm	# KS<0.1	Q1	Q2	Q3
8-schools	F-T F-T	10	15011	15316	15506
8-schools	V-T* F-T	10	11088	11290	11698
8-schools	V-T* F-T*	10	10767	11222	12074
8-schools	V-T*-F	10	19047	20811	22046
coll-rockets	F-T F-T	10	11323	12013	12700
coll-rockets	V-T* F-T	10	12799	13358	14301
coll-rockets	V-T* F-T*	10	12315	12829	13350
coll-rockets	V-T*-F	10	23473	24712	27128
mining	F-T F-T	10	22004	23410	24588
mining	V-T* F-T	10	22136	24382	24928
mining	V-T* F-T*	10	22111	22799	23663
mining	V-T*-F	10	31719	33186	33899
mrna-no-transf	F-T F-T	9	2180	2360	2709
mrna-no-transf	V-T* F-T	7	2755	2783	3013
mrna-no-transf	V-T* F-T*	10	2688	2816	2881
mrna-no-transf	V-T*-F	10	4787	5053	5350
phylo	F-T F-T	10	13061	14249	16406
phylo	V-T* F-T	10	14256	15036	15927
phylo	V-T* F-T*	10	13798	14476	15071
phylo	V-T*-F	10	21723	24421	25046
sparse-car	F-T F-T	10	6945	7071	7372
sparse-car	V-T* F-T	10	6234	6777	7817
sparse-car	V-T* F-T*	10	6122	6853	7460
sparse-car	V-T*-F	10	13244	14351	15011
titanic	F-T F-T	10	16942	17567	18469
titanic	V-T* F-T	9	20082	20601	21078
titanic	V-T* F-T*	10	19982	20406	20871
titanic	V-T*-F	10	29952	31216	33741
toy-mix	F-T F-T	10	1766	1843	1936
toy-mix	V-T* F-T	9	3186	3347	3631
toy-mix	V-T* F-T*	10	3093	3195	3307
toy-mix	V-T*-F	10	5942	6129	6296
vaccines	F-T F-T	10	28148	30611	32884
vaccines	V-T* F-T	10	26536	29297	31160
vaccines	V-T* F-T*	10	29905	31443	33514
vaccines	V-T*-F	10	34517	35911	38177

Table 3: Quantiles (0.25, 0.5, 0.75) of the ESS for the subset of the runs with KS < 0.1.

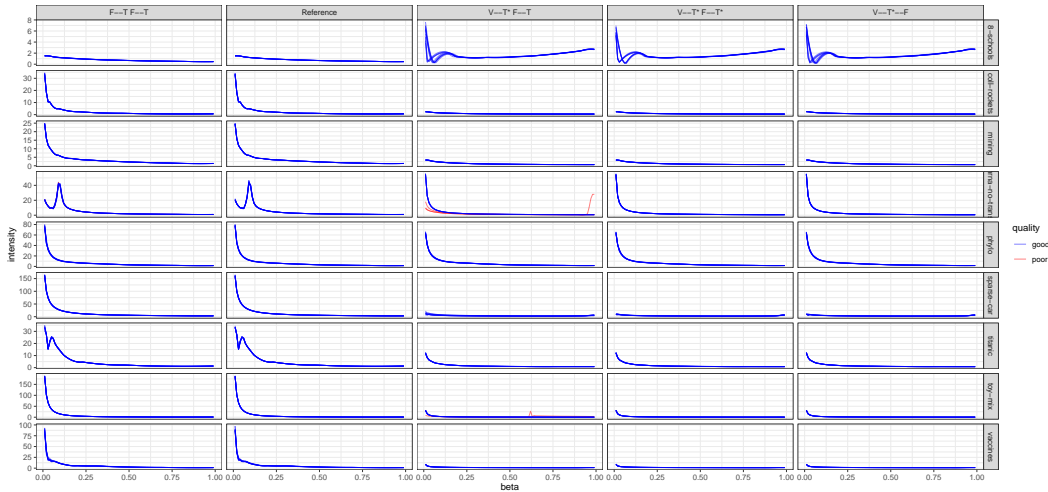


Figure 17: The local communication barrier for nine models (row). For the variational methods, the plot shows the local communication barrier between the variational distribution and the target; for standard PT, the plot shows the local communication barrier between the fixed reference and the target. We show the estimated functions for the five algorithms (columns) and ten random seeds. Red curves indicate “catastrophic failures” as described in Fig. 2.

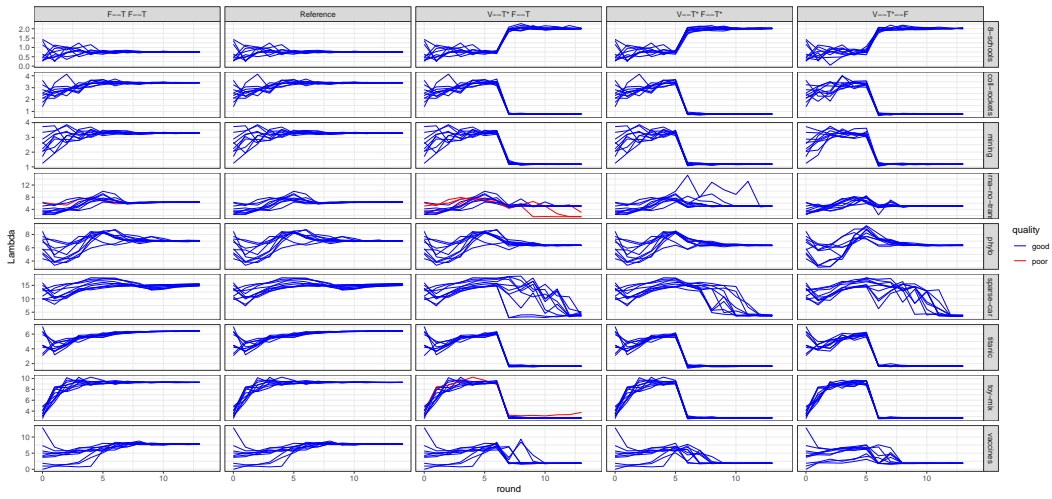


Figure 18: The global communication barrier estimates between the reference and target distributions for nine models (row), each shown as a function of the adaptation round. For the variational methods, the plot shows the global communication barrier between the variational distribution and the target; for standard PT, the global communication barrier is computed between the fixed reference and the target. We show the estimated communication barriers for the five algorithms (columns) and ten random seeds. Red curves indicate “catastrophic failures” as described in Fig. 2.